SIAM J. Applied Dynamical Systems
Vol. 10, No. 2, pp. 423–451

Nondeterministic Chaos, and the Two-fold Singularity in Piecewise Smooth Flows*

Alessandro Colombo† and Mike R. Jeffrey‡

Abstract. A vector field is piecewise smooth if its value jumps across a hypersurface, and a two-fold singularity is a point where the flow is tangent to the hypersurface from both sides. Two-folds are generic in piecewise smooth systems of three or more dimensions. We derive the local dynamics of all possible two-folds in three dimensions, including nonlinear effects around certain bifurcations, finding that they admit a flow exhibiting chaotic but nondeterministic dynamics. In cases where the flow passes through the two-fold, upon reaching the singularity it is unique in neither forward nor backward time, meaning the causal link between inward and outward dynamics is severed. In one scenario this occurs recurrently. The resulting flow makes repeated, but nonperiodic, excursions from the singularity, whose path and amplitude is not determined by previous excursions. We show that this behavior is robust and has many of the properties associated with chaos. Local geometry reveals that the chaotic behavior can be eliminated by varying a single parameter: the angular jump of the vector field across the two-fold.

Key words. two-fold, sliding, Filippov, nondeterminism, chaos, bifurcation

AMS subject classifications. 34C23, 37G10, 37G35

DOI. 10.1137/100801846

1. Introduction.

Piecewise smooth vector fields have appeared throughout the history of dynamical systems as models of mechanical and electronic devices (e.g., [1]) and, more recently, have seen growing use in fields such as ecology, economics, and neuroscience. Their spreading use has naturally been accompanied by interest in their generic mathematical and dynamical properties, which have been the subject of a number of recent books (e.g., [10,18,22,32]). Their dynamics were formalized by Filippov [14], using differential inclusions (set-valued differential equations; see [3]) to overcome the problem of indefiniteness of the vector field on the surfaces of discontinuity.

Although two-dimensional piecewise smooth systems are now rather well understood (see, for example, [14, 21]), a general understanding of dynamics in three or more dimensions is crucially obstructed by the appearance of the so-called *two-fold* singularity [30]. The two-fold is a simple topological singularity that is generic in piecewise smooth systems with three or more dimensions. This implies that it may well be commonplace in systems of a piecewise smooth nature. Contrarily, two-folds are neither well known nor well understood, with regard to either the theory of their dynamics or the frequency of their appearance in physical systems.

*Received by the editors July 13, 2010; accepted for publication (in revised form) by H. Kokubu March 1, 2011; published electronically May 26, 2011.
http://www.siam.org/journals/siads/10-2/80184.html
†Department of Electronics and Information, Via Ponzio 34/5, 20133 Milano, Italy (alessandro.colombo@polimi.it).
‡Engineering Mathematics Department, Queen's Building, University of Bristol, BS8 1TR, Bristol UK (mike.jeffrey@bris.ac.uk). The work of this author was supported by the EPSRC grant Making It Real.

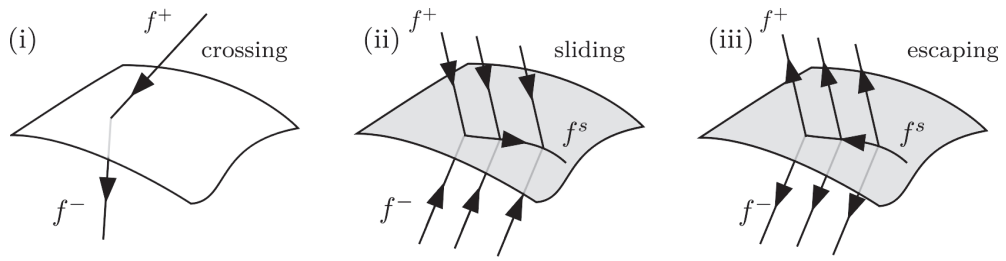

Figure 1. *Dynamics at a switching manifold in a three-dimensional piecewise smooth system. The vector field switches between f^+ and f^-. An orbit meeting the manifold may either:* (i) *cross through it,* (ii) *reach it in finite time and then follow the sliding vector field f^s, or* (iii) *escape it in finite time, though it may slide along the manifold for some time before escaping.*

The purpose of this paper is to present, in an organic and consistent framework, all existing results regarding the local dynamics near the two-fold. This also includes some novel results about particular forms of the two-fold that reveal its role in the sudden onset of periodic orbits and recurrent nondeterministic dynamics.

The two-fold was already well defined in [14]. In a piecewise smooth vector field, discontinuities are assumed to occur across a hypersurface called the *switching manifold*. Since it is a hypersurface, we can speak of the manifold as locally having two sides, and generically there may exist points where the vector field is quadratically tangent to one side of the manifold or the other. We call such a tangency a *fold*, because in the projection along the flow the switching manifold has a simple fold. This assumes the system to be at least two-dimensional. In higher dimensions there may generically exist points where two folds intersect transversely, so that the vector field is tangent to both sides of the manifold, and this simple object is a *two-fold*. A two-fold is an important organizing center because it brings together all of the basic forms of dynamics possible in a piecewise smooth system. Filippov [14] described three basic forms of dynamics that would occur at a switching manifold: crossing, sliding, and escaping, depending on the orientation of the vector field either side of the switching manifold, as illustrated in Figure 1. Crossing, shown in Figure 1(i), occurs where the component of the vector field normal to the switching manifold has the same direction on both sides. In the two other cases the normal component of the vector field switches direction, so that the vector field is either directed towards the switching manifold, giving sliding as in (ii), or is directed away from the manifold, giving escaping as in (iii).

At a fold (see Figure 2) the vector field on one side of the switching manifold changes its normal direction, forming a boundary between crossing regions and sliding or escaping regions. At a two-fold, the vector fields either side of the manifold both change their normal direction, meaning that regions of all three dynamical behaviors—crossing, sliding, and escaping—meet, and their boundaries intersect to form the singularity.

Escaping dynamics (see Figure 1(iii)) is typically neglected on the basis that it simply constitutes a time-reversal of sliding, and that escaping regions cannot be reached by a system in forward time, making consequences of forward time nonuniqueness in these regions irrelevant [10, 11, 27]. This assumption is incorrect at a two-fold, which can channel sliding dynamics into the escaping region. This gives whole families of orbits robust access to regions

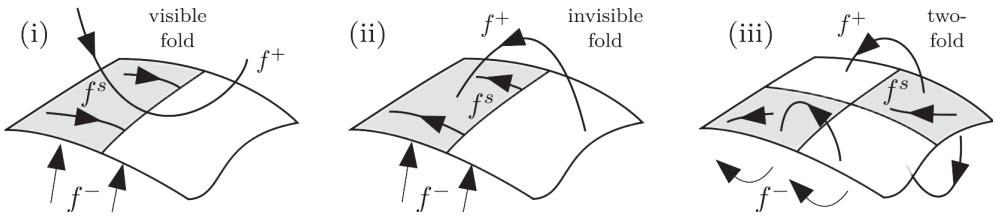

Figure 2. *Tangencies in a piecewise smooth system, showing:* (i) *a visible fold,* (ii) *an invisible fold; these form the boundaries between sliding (shaded) and crossing (unshaded) (reverse arrows to replace sliding with escaping).* (iii) *Folds associated with the upper and lower fields cross to form a two-fold, where both vector fields are tangent to the switching manifold (in the case illustrated, both folds are invisible).*

of phase space that are infinitely repelling. This counterintuitive dynamical behavior, noticed in Filippov's seminal work [14], seems to have been overlooked ever since, though a similar effect was discovered in the framework of nonstandard analysis [4] as the so-called canard phenomenon. Canards are now a popular topic in singular perturbation theory [13, 28], with numerous applications, of which a few examples are in neuron modelling [24], chemical dynamics [6, 26], gas pressure dynamics [5], and ecology [9]. Despite qualitative similarities in these approaches, their connection to the two-fold is as poorly understood as the two-fold itself. These connections are not the subject of this paper, and we restrict our interest to understanding the two-fold in the context of generic piecewise smooth dynamical systems.

The study of dynamics around a two-fold has been mainly limited to a lowest order approximation in three dimensions [14, 16, 29, 30]. Such local analysis reveals how an initially smooth flow far from a discontinuity can evolve toward a state where its forward evolution is set-valued. In this paper we review these results and extend them by carrying out a comprehensive analysis of the nonlinear behavior of two-folds in three dimensions. In so doing, we determine the invariant sets that are present near the two-fold and decode their complex dynamics.

In section 2 we define the two-fold singularity and its three types. We discuss the first of these, the invisible two-fold, or *Teixeira singularity*, in detail in section 3; we analyze its sliding and crossing dynamics separately in sections 3.1 and 3.2, using them to reconstruct the full system in sections 3.3 and 3.4. We briefly discuss the other forms, the visible (short for visible-visible) two-fold in section 4, and the visible-invisible two-fold in section 5, with a remark on their bifurcations in section 6. In section 7 we numerically simulate some particularly interesting dynamics predicted in section 3, with some closing remarks in section 8.

2. The three flavors of two-fold. Consider a three-dimensional piecewise smooth system of ordinary differential equations

$$\dot{\mathbf{x}} = f^+(\mathbf{x}) \quad \text{when } h(\mathbf{x}) > 0, \qquad \dot{\mathbf{x}} = f^-(\mathbf{x}) \quad \text{when } h(\mathbf{x}) < 0, \tag{2.1}$$

where the dot denotes differentiation with respect to time $t \in \mathbb{R}$ and where $h(\mathbf{x})$ is a regular scalar function of the state vector $\mathbf{x} = (x_0, x_1, x_2) \in \mathbb{R}^3$. For simplicity we set $h(\mathbf{x}) = x_0$, since any piecewise smooth system, in a region where $h(\mathbf{x}) = 0$ defines a manifold, can be put into this form through the appropriate change of variables [14, 30]. Then, $x_0 = 0$ is the switching manifold. Following Filippov's definition [14], the solution of (2.1) at the switching manifold

includes all solutions of the differential inclusion

$$\dot{\mathbf{x}} \in f := f^- + \lambda(f^+ - f^-), \tag{2.2}$$

where $\lambda = 0$ when $h(x) < 0$, $\lambda = 1$ when $h(x) > 0$, and $\lambda \in [0,1]$ when $h(x) = 0$, so that f is a set-valued convex combination of f^+ and f^- where $h(x) = 0$. In practice, when the components of f^+ and f^- normal to the switching manifold have opposite direction, f admits a solution that lies on the switching manifold and satisfies the system given by

$$\dot{\mathbf{x}} = f^s(\mathbf{x}) \quad \text{when } x_0 = 0, \tag{2.3}$$

where the *sliding vector field*, f^s, is defined as

$$f^s = f^- + \frac{\mathcal{L}_{f^-}h}{\mathcal{L}_{f^-}h - \mathcal{L}_{f^+}h}(f^+ - f^-). \tag{2.4}$$

The symbol $\mathcal{L}_f$ denotes the Lie derivative along the flow of a field f, given by $\mathcal{L}_f = f \cdot \nabla = \dot{\mathbf{x}} \cdot \frac{d}{d\mathbf{x}}$. Let $\mathcal{L}_f^2$ denote the second Lie derivative $\mathcal{L}_f^2 = (\mathcal{L}_f)^2$. The dynamics in a general piecewise smooth system is then a composite of the dynamics of f^+, f^-, and f^s. We make the following distinctions.

Definition of orbits and flow. An *orbit segment* is any smooth path $\mathbf{x} = \mathbf{x}(t)$ satisfying (2.2), entirely contained in one of the regions $\{\mathbf{x} : h(\mathbf{x}) > 0\}$, $\{\mathbf{x} : h(\mathbf{x}) < 0\}$, or $\{\mathbf{x} : h(\mathbf{x}) = 0\}$. An *orbit* is any continuous path $\mathbf{x}(t)$ that satisfies (2.2), formed by concatenating orbit segments. The *flow of* (2.2) through a point $\hat{\mathbf{x}}$ at time t is given by all points $\mathbf{x}(t+\tau)$ with $\mathbf{x}(\tau) = \hat{\mathbf{x}}$ for some $\tau \in \mathbb{R}$, $\mathbf{x}(t)$ satisfying (2.2). In the following, by the flow we mean the flow of (2.2) unless otherwise stated.

An important consequence of this definition is that the flow through a point $\hat{\mathbf{x}}$ in a sliding region is not unique, because $\hat{\mathbf{x}}$ always belongs to a one-parameter family of orbits (unless it is an equilibrium). For example, the six orbits shown in Figure 1(ii) each overlap in the sliding region, so through any point $\hat{\mathbf{x}}$ on the overlap the flow is nonunique; the same applies to the six orbits shown in Figure 1(iii).

Now let us assume that both f^+ and f^- have quadratic contact with the switching manifold at the origin, that is,

$$\mathcal{L}_{f^+}h(0) = 0 \quad \text{and} \quad \mathcal{L}_{f^+}^2 h(0) \neq 0, \tag{2.5a}$$

$$\mathcal{L}_{f^-}h(0) = 0 \quad \text{and} \quad \mathcal{L}_{f^-}^2 h(0) \neq 0. \tag{2.5b}$$

Let us also require that neither f^+ nor f^- has equilibria near the origin,

$$f^+ \neq 0 \quad \text{and} \quad f^- \neq 0, \tag{2.6}$$

and that the pair of curves given by $\mathcal{L}_{f^+}h = 0$ and $\mathcal{L}_{f^-}h = 0$ on $h = 0$ intersect transversely at the origin,

$$\det\left(\nabla h(0),\ \nabla\mathcal{L}_{f^+}h(0),\ \nabla\mathcal{L}_{f^-}h(0)\right) \neq 0. \tag{2.7}$$

A point satisfying either (2.5a) or (2.5b) on $x_0 = 0$ is a *fold*. A point satisfying both conditions (2.5), and also satisfying the nondegeneracy conditions (2.6)–(2.7), is a *two-fold*.

The sign of the second Lie derivative determines whether a fold is visible, meaning the vector field curves away from the switching manifold because $\mathcal{L}^2_{f^+}h(0) > 0$ or $\mathcal{L}^2_{f^-}h(0) < 0$, or invisible, meaning the vector field curves towards the switching manifold because $\mathcal{L}^2_{f^+}h(0) < 0$ or $\mathcal{L}^2_{f^-}h(0) > 0$. These are illustrated in Figure 2(i) and (ii). If at least one fold is visible, the dynamics is relatively easy to analyze, and these cases, which we call the visible and visible-invisible two-folds, are discussed in sections 4–5. If both folds are invisible, then the flows of f^+ and f^- both map orbits repeatedly back to the switching manifold, and the dynamics is rather more rich, earning this invisible two-fold the distinguished name of a Teixeira singularity (after the author of [30], who brought this singularity to prominence). Therefore the Teixeira singularity is our main subject of interest.

3. The Teixeira singularity. In this section we begin by summarizing a linear approximation of the Teixeira singularity previously studied in [14,16,30]. In particular, (3.1)–(3.6) and (3.8)–(3.11) summarize results obtained in [16]. In the remainder of section 3 we introduce higher order terms to the approximation, which unfold the bifurcation found in [16].

Following on from section 2, local to a two-fold where $\mathcal{L}^2_{f^+}h(0) < 0$ and $\mathcal{L}^2_{f^-}h(0) > 0$, the system (2.1) can be simplified by two changes of variables and a time rescaling. (For a lengthier description than we give below, see [16].) First, given (2.7), we can make a smooth coordinate transformation that places the folds associated with f^- and f^+ along the x_1 and x_2 axes, respectively. Then, by rescaling x_1 and x_2, and rescaling time separately above and below the switching manifold—this changes the speed of the trajectories of f^+ and f^- but preserves both of their phase portraits as well as that of f^s—we arrive at the local form near the origin:

$$f^+ = \begin{pmatrix} -x_1 + \mathcal{O}(x_0, \|x_1, x_2\|^2) \\ 1 \ + \mathcal{O}(\|\mathbf{x}\|) \\ V^+ + \mathcal{O}(\|\mathbf{x}\|) \end{pmatrix}, \tag{3.1a}$$

$$f^- = \begin{pmatrix} x_2 + \mathcal{O}(x_0, \|x_1, x_2\|^2) \\ V^- + \mathcal{O}(\|\mathbf{x}\|) \\ 1 \ + \mathcal{O}(\|\mathbf{x}\|) \end{pmatrix}, \tag{3.1b}$$

where $V^\pm$ are real constants. Geometrically, V^+ (respectively, V^-) measures the cotangent of the angle θ^+ (θ^-) between the vector field f^+ (f^-) and its fold line $\mathcal{L}_{f^+}h|_{x_0=0} = 0$ ($\mathcal{L}_{f^-}h|_{x_0=0} = 0$). These can be retrieved for a general vector field at a Teixeira singularity from the formulae

$$V^+ = \cot\theta^+ = \frac{\mathcal{L}_{f^+}\mathcal{L}_{f^-}h}{\sqrt{-(\mathcal{L}^2_{f^+}h)(\mathcal{L}^2_{f^-}h)}}, \tag{3.2a}$$

$$V^- = \cot\theta^- = \frac{-\mathcal{L}_{f^-}\mathcal{L}_{f^+}h}{\sqrt{-(\mathcal{L}^2_{f^+}h)(\mathcal{L}^2_{f^-}h)}}, \tag{3.2b}$$

evaluated at the two-fold.

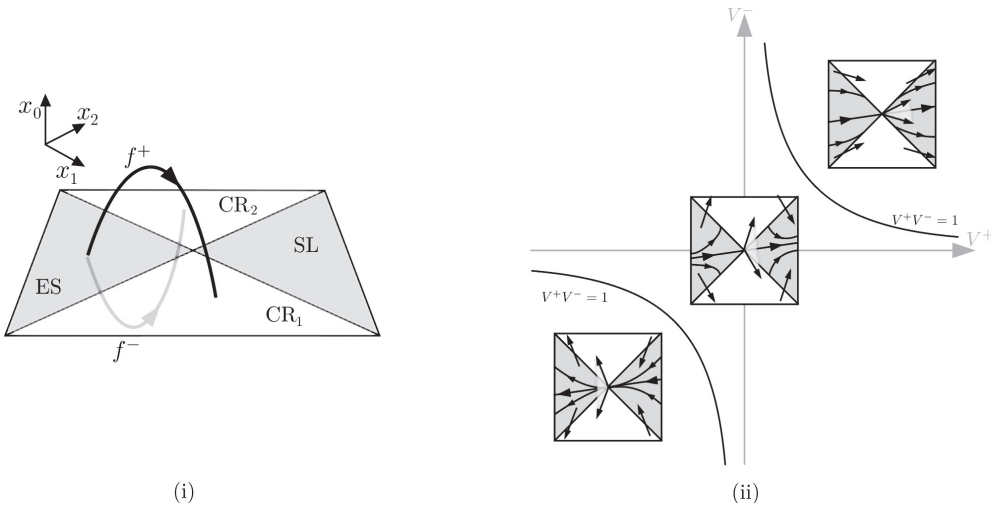

Figure 3. *Dynamics near a Teixeira singularity:* (i) *orbits outside the switching manifold curve around the folds and cross the manifold in CR_1 and CR_2,* (ii) *phase portraits of the sliding dynamics. At the origin the sliding vector field f^s is set-valued, with elements pointing into the escaping region ES when $V^+V^- > 1$ and $V^+, V^- < 0$. In this case a one-parameter family of orbits intersects the origin along a unique direction (an eigenvector of $\tilde{f}^s$ from (3.4)). In all other cases the set-valued f^s has elements which point into the sliding region SL, and only a single orbit that intersects the singularity.*

The dynamics of (3.1) is illustrated in Figure 3(i) and is at first glance very simple. The flow of f^+ maps initial points from the region $\{x_0 = 0, x_1 < 0\}$ to the region $\{x_0 = 0, x_1 > 0\}$, affecting a reflection ϕ^+ in the plane $x_1 = 0$ along the direction $(0, 1, V^+) + \mathcal{O}(\|\mathbf{x}\|)$. Likewise, the flow of f^- maps initial points from the region $\{x_0 = 0, x_2 < 0\}$ to the region $\{x_0 = 0, x_2 > 0\}$, affecting a reflection ϕ^- in the plane $x_2 = 0$ along the direction $(0, V^-, 1) + \mathcal{O}(\|\mathbf{x}\|)$.

The switching manifold is divided into quadrants as illustrated in Figure 3: the *sliding region* $\{x_0 = 0, x_1 > 0, x_2 > 0\}$ (SL in Figure 3), the *escaping region* $\{x_0 = 0, x_1 < 0, x_2 < 0\}$ (ES in Figure 3), and the *crossing regions* $\{x_0 = 0, x_1 x_2 < 0\}$ (CR_1 and CR_2 in Figure 3), separated by the folds. In each crossing region, CR_1 and CR_2, the dynamics can be analyzed by a second return map, the concatenation of the maps ϕ^+ and ϕ^-. A sequence of crossings will terminate in forward time if it maps into the sliding region SL, where both f^+ and f^- point toward the switching manifold. Conversely it has initial points in the escaping region ES, where both vector fields point away from the manifold.

Through CR_1 and CR_2 the flow is continuous and invertible, but orbits have vertices where they traverse the switching manifold. The flow through any point in SL is defined uniquely in forward time and contains a segment of sliding, but in reverse time it consists of an infinite number of orbits arriving from $x_0 > 0$ and $x_0 < 0$, and hence the flow is set-valued in reverse time. In ES the flow is defined uniquely in reverse time, but in forward time it is set-valued, generating an infinity of orbits that escape into $x_0 > 0$ and $x_0 < 0$.

Thus we can study the flow around the singularity in terms of two dynamical systems on the switching manifold: (i) continuous-time dynamics of sliding orbit segments, which are solutions of f^s in SL and ES and which live in the two-dimensional switching manifold, and (ii)

discrete-time dynamics of crossing orbit segments, which wind around the singularity inducing a return map on the switching manifold. In the next two sections we analyze these separately and can restrict our analysis to the x_1-x_2 plane. We reassemble the three-dimensional dynamics in section 3.3.

3.1. Dynamics in the sliding and escaping regions. Evaluating (3.1) at $x_0 = 0$, and substituting into (2.4), we obtain the explicit expression for the sliding vector field:

$$f^s = \begin{pmatrix} 0 \\ \dfrac{V^- x_1 + x_2 + \mathcal{O}(\|x_1, x_2\|^2)}{d(\mathbf{x})} \\ \dfrac{x_1 + V^+ x_2 + \mathcal{O}(\|x_1, x_2\|^2)}{d(\mathbf{x})} \end{pmatrix}, \tag{3.3}$$

where $d(\mathbf{x}) = x_1 + x_2 + \mathcal{O}(\|x_1, x_2\|^2)$. This vector field is undefined at the origin since, f^+ and f^- both being tangent to the switching manifold at 0, all vectors in their convex combination are tangent to the switching manifold. To overcome this, following [14,30], we define a planar regularized vector field, $\tilde{f}^s$, by multiplying f^s by $d(\mathbf{x})$ and omitting the trivial x_0 component,

$$\tilde{f}^s(x_1, x_2) = \begin{pmatrix} V^- & 1 \\ 1 & V^+ \end{pmatrix} \begin{pmatrix} x_1 \\ x_2 \end{pmatrix} + \mathcal{O}(\|x_1, x_2\|^2). \tag{3.4}$$

Because $d(\mathbf{x}) > 0$ in SL and $d(\mathbf{x}) < 0$ in ES, $\tilde{f}^s$ and f^s have the same phase portrait in the SL, but the same phase portrait with time reversed in ES. Additionally, because $d(0) = 0$, $\tilde{f}^s$ has an equilibrium at the origin, where (3.3) is not well defined. These facts are vital to take into account when translating the dynamics of $\tilde{f}^s$ into those of the original vector field f^s. The equilibrium of $\tilde{f}^s$ at the origin has eigenvalues

$$\mu_\pm = \frac{1}{2}\left(V^+ + V^- \pm \sqrt{(V^+ - V^-)^2 + 4}\right), \tag{3.5}$$

and the associated eigenvectors are

$$\begin{pmatrix} \mu_\pm - V^+ \\ 1 \end{pmatrix}. \tag{3.6}$$

If the eigenvalue μ_i has negative (respectively, positive) real part, we say it and its associated eigenvector are stable (unstable). Some simple calculations show that one eigenvector lies always in SL and ES, and the other lies in CR_1 and CR_2; they can never be tangent to either of the folds since this would correspond to a cubic tangency of f^+ or f^- at the origin (called a *cusp* point), excluded by (2.5). In particular,

(i) if $V^+, V^- < 0$ and $V^+V^- > 1$, both eigenvectors are stable;
(ii) if $V^+V^- < 1$, the eigenvector in SL/ES is unstable and the other is stable;
(iii) if $V^+, V^- > 0$ and $V^+V^- > 1$, both eigenvectors are unstable.

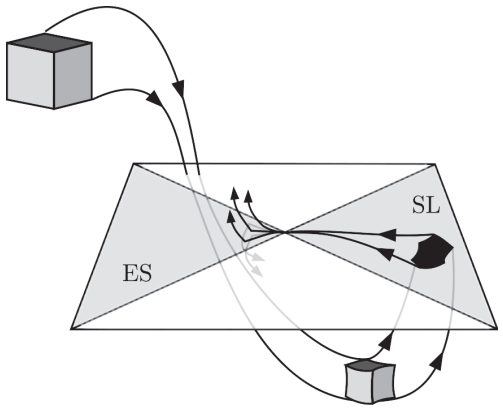

Figure 4. *An illustration of nondeterminism at the Teixeira singularity. Orbits which are initially smooth evolve toward a switching manifold, eventually enter the sliding region SL, and evolve toward the singularity. Open sets of initial conditions thus evolve through the singularity in finite time and are ejected as a one-parameter family of orbits in the escaping region ES.*

Moreover, when the eigenvector in SL/ES is stable, it is associated with the weak stable eigenvalue, so that sliding orbit segments are asymptotically attracted to it as they approach the singularity.

The different cases are illustrated in Figure 3(ii). Referring to the *definition of orbits and flow* in section 2, the phase portraits in Figure 3(ii) imply that in case (i) orbits cross the singularity from SL to ES, while in cases (ii)–(iii) orbits cross from ES to SL. In each case orbits cross the two-fold singularity in finite time. In case (i) in particular, orbits with an initial interval of smooth evolution away from the discontinuity can enter SL and evolve toward the singularity (Figure 4), whereupon their forward evolution is multivalued. Importantly, such orbits reach the singularity in finite time, and as they cross it all information about their initial conditions is lost. By this mechanism, forward time uniqueness is lost for orbits that converge on the singularity. One purpose of the present paper is to reveal the dynamical implications of this often overlooked loss of uniqueness.

We can determine whether f^s is structurally stable by considering $\tilde{f}^s$. The Jacobian of (3.4) at 0 is singular when $V^+V^- = 1$, and a quick inspection of (3.1) shows that this corresponds to f^+ and f^- being antiparallel (if $V^+, V^- < 0$) or parallel (if $V^+, V^- > 0$) at the origin. The eigenvector $(-V^+, 1)$, associated with $\mu_- = 0$, always points into SL if $V^+, V^- < 0$ and into one of the crossing regions CR_1 or CR_2 if $V^+, V^- > 0$. Only the case when $V^+, V^- < 0$ results in a structurally unstable phase portrait of the sliding vector field when $V^+V^- = 1$. In this case, the behavior of the orbits of $\tilde{f}^s$ around the origin is captured by the dynamics in the one-dimensional center manifold with Taylor expansion

$$\dot{u} = (V^+V^- - 1)u + a_2u^2 + \mathcal{O}(u^3), \tag{3.7}$$

which exhibits a transcritical bifurcation at $V^+V^- = 1$ (details about this normal form are given in Appendix A). Notice that, for f^s, this means that there exists a single equilibrium that crosses the singularity when $V^+V^- = 1$, changing stability in the process. Since equilibria of the sliding vector field f^s are not zeros of f^+ or of f^-, they are commonly called

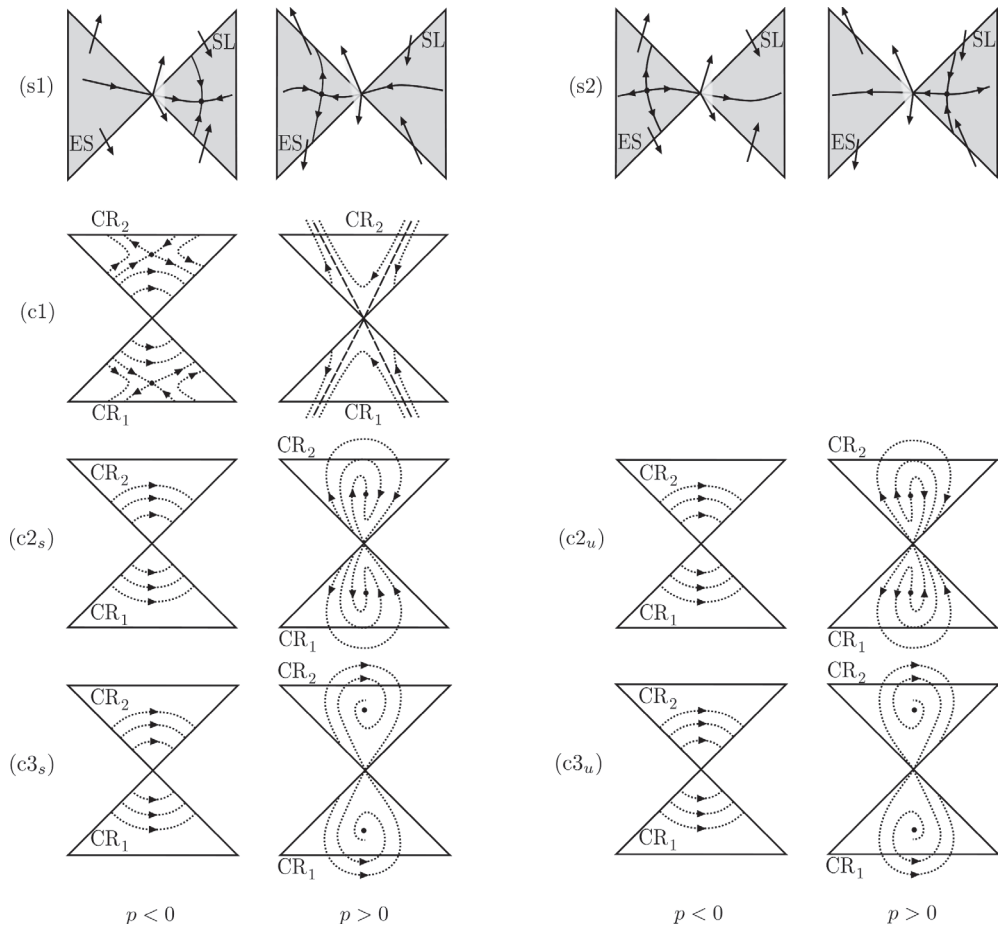

Figure 5. *The complete catalogue of local dynamics around a Teixeira singularity when* $p = V^+V^- - 1 \simeq 0$ *is obtained by composing the possible phase portraits of sliding* (s1), (s2), *and crossing* (c1), ($c2_{s,u}$), ($c3_{s,u}$). (s1), (s2) *show the two possible phase portraits in the sliding and escaping regions SL and ES as the bifurcation parameter p changes sign.* (c1), ($c2_{s,u}$), ($c3_{s,u}$) *depict the intersections of orbits with the crossing regions* CR_1 *and* CR_2 *as p changes sign. (These are derived from the unfoldings in* [12].*) The crossing maps in* ($c2_s$) *and* ($c3_s$) *have a stable fixed point of node and focus type, respectively, while the dual cases in* ($c2_u$) *and* ($c3_u$) *have unstable fixed points. Altogether, composing cases* (s1), (s2) *with cases* (c1), ($c2_{s,u}$), ($c3_{s,u}$), *ten qualitatively different portraits are obtained.*

pseudoequilibria [15]. Assuming that the positive u semiaxis lies in SL, the pseudoequilibrium of f^s is one of the following:

(s1) if $a_2 > 0$ in (3.7), a saddle in ES for $V^+V^- > 1$ and $V^+, V^- < 0$, becoming a stable node in SL when $V^+V^- < 1$ or $V^+, V^- > 0$;

(s2) if $a_2 < 0$ in (3.7), a saddle in SL for $V^+V^- > 1$ and $V^+, V^- < 0$, becoming an unstable node in ES when $V^+V^- < 1$ or $V^+, V^- > 0$.

These are illustrated in Figure 5.

3.2. Dynamics in the crossing regions. In the crossing regions CR_1 and CR_2, orbit segments of f^+ and f^- induce maps ϕ^+ and ϕ^- from the switching manifold to itself, across

the folds. The vector fields (3.1) truncated to lowest order are easily integrated to obtain the maps

$$\tilde{\phi}^+ : \mathbb{R}^- \times \mathbb{R} \mapsto \mathbb{R}^+ \times \mathbb{R} = \begin{pmatrix} -1 & 0 \\ -2V^+ & 1 \end{pmatrix} \begin{pmatrix} x_1 \\ x_2 \end{pmatrix} + \mathcal{O}(\|x_1, x_2\|^2) \tag{3.8a}$$

and

$$\tilde{\phi}^- : \mathbb{R} \times \mathbb{R}^- \mapsto \mathbb{R} \times \mathbb{R}^+ = \begin{pmatrix} 1 & -2V^- \\ 0 & -1 \end{pmatrix} \begin{pmatrix} x_1 \\ x_2 \end{pmatrix} + \mathcal{O}(\|x_1, x_2\|^2). \tag{3.8b}$$

The full maps ϕ^+ and ϕ^-, whose Taylor expansions to the third order are reported in Appendix B, are then retrieved as generic perturbations of these, by imposing that they preserve the corresponding fold lines and are involutions (since a map in the neighborhood of a fold is an involution; see, e.g., [2]).

To understand the dynamics of orbits that wind around the singularity, crossing through CR_1 and CR_2, we can study their Poincaré map from a crossing region (either CR_1 or CR_2) back to itself; this map is obtained as a composition of ϕ^+ and ϕ^-. Let us consider the map $\phi = \phi^+ \circ \phi^-$ (similar arguments follow if we choose instead the map $\phi^- \circ \phi^+$). The domain of ϕ is the set $D \subseteq \mathrm{CR}_1$ such that $\phi^-(D) \subseteq \mathrm{CR}_2$. Orbits with initial conditions in D cross through CR_2 and return to CR_1 or SL. The complement of D in CR_1 consists of initial conditions that are mapped into SL by ϕ^-. This implies that D lies between the negative x_2 axis and the preimage of the positive x_2 axis under the map ϕ^-; since ϕ^- is an involution, the preimage is a curve given by $\phi^-(x_1 = 0, x_2 > 0)$. The Poincaré map thus obtained is

$$\phi : \begin{pmatrix} x_1 \\ x_2 \end{pmatrix} \mapsto \begin{pmatrix} -1 & 2V^- \\ -2V^+ & 4V^+V^- - 1 \end{pmatrix} \begin{pmatrix} x_1 \\ x_2 \end{pmatrix} + \mathcal{O}(\|x_1, x_2\|^2). \tag{3.9}$$

This map has a fixed point at the origin, with eigenvalues

$$\lambda_\pm = 2V^+V^- - 1 \pm 2\sqrt{V^+V^-(V^+V^- - 1)}. \tag{3.10}$$

When $V^+V^- > 1$ or $V^+V^- < 0$ the fixed point is of saddle type. When $0 < V^+V^- < 1$ it is a center, with complex conjugate eigenvalues on the unit circle. The corresponding eigenvectors are

$$\begin{pmatrix} 2V^- \\ 1 + \lambda_\pm \end{pmatrix}. \tag{3.11}$$

As long as $V^+V^- < 1$ or $V^+, V^- > 0$, it was proved in [16] that all orbits sufficiently close to the singularity reach SL after a finite number of crossings. A bifurcation of the crossing dynamics occurs when $V^+V^- = 1$ and $V^+, V^- < 0$. At the bifurcation, the Jacobian of the Poincaré map at the origin is nonsemisimple (nondiagonalizable) and has two eigenvalues equal to 1. As a consequence of ϕ^+ and ϕ^- being involutions, this corresponds to a degenerate 1:1 resonance bifurcation of the map. Near the bifurcation, the map can be reduced to the normal form

$$\begin{aligned} u_1 &\mapsto u_1 + u_2 + \mathcal{O}(\|\mathbf{u}\|^4), \\ u_2 &\mapsto 4pu_1 + (1 + 4p)u_2 + B_{11}u_1u_2 + B_{30}u_1^3 + B_{21}u_1^2u_2 + B_{03}u_2^3 + \mathcal{O}(\|\mathbf{u}\|^4), \end{aligned} \tag{3.12}$$

with

$$p = V^+V^- - 1, \tag{3.13}$$

through a series of changes of variables and parameters which are reported in Appendix C. At the bifurcation and at the origin, the u_1 axis lies along the vector direction $(V^-, 1)$, the singular eigenvector of the Jacobian of ϕ, and the positive direction of u_1 points into CR_2, while the u_2 axis is tangent to the x_1 axis in the original coordinates. The normal form has a fixed point at the origin for all values of p, while two more fixed points, located at

$$u_1 = \pm 2\sqrt{-\frac{p}{B_{30}}}, \qquad u_2 = 0, \tag{3.14}$$

emerge when $-p/B_{30}$ becomes positive. The positivity of the eigenvalues (3.10) implies that the negative u_1 axis intersects CR_1 and lies inside the domain of the Poincaré map ϕ, implying that the fixed point at $u_1 = -2\sqrt{-p/B_{30}}$ corresponds to a crossing periodic orbit near the singularity. The eigenvalues of this fixed point are

$$1 - B_{11}\sqrt{-\frac{p}{B_{30}}} \pm \sqrt{-\frac{p}{B_{30}}(8B_{30} + B_{11}^2)} + \mathcal{O}(p). \tag{3.15}$$

Depending on the values of B_{11} and B_{30}, the following are possible:

(c1) if $B_{30} > 0$, the two eigenvalues are real, one positive and one negative;
(c2) if $B_{30} < 0$ and $|8B_{30}| < B_{11}^2$, both eigenvalues are real, inside the unit circle if $B_{11} > 0$, outside the unit circle otherwise;
(c3) if $B_{30} < 0$ and $|8B_{30}| > B_{11}^2$, the eigenvalues are complex conjugate, inside the unit circle if $B_{11} > 0$, outside otherwise.

The orbits of map (3.12) are approximated, for $p = 0$, by the unit-time shift of a flow which is equivalent to

$$\begin{aligned} \dot{\nu}_1 &= \nu_1 + \mathcal{O}(\|\nu\|^4), \\ \dot{\nu}_2 &= B_{11}\nu_1\nu_2 + B_{30}\nu_1^3 + \left(\frac{B_{11}^2}{2} + B_{21} - 3B_{30}\right)\nu_1^2\nu_2 + \mathcal{O}(\|\nu\|^4), \end{aligned} \tag{3.16}$$

as explained in Appendix D. This degenerate (codimension-three) Bogdanov–Takens normal form is discussed in [19], and it is unfolded in three parameters in [12]. In our case, changing p around 0, we explore a one-dimensional curve of parameters through the three-dimensional unfolding. In [12] the cases (c1), (c2), (c3) are called respectively the saddle, elliptic, and focus cases, after the topological type of the origin when $p = 0$. Overall, cases (c1), (c2), (c3) give rise to the following bifurcation scenarios of the crossing dynamics in a neighborhood of the origin:

(c1) For $p > 0$ the singularity is a saddle of the map ϕ. For $p < 0$ a saddle cycle emerges from the singularity, and the singularity is a center of the map ϕ.
(c2) For $p < 0$ the singularity is a center of the map ϕ. For $p > 0$ a node cycle emerges from the singularity, and the singularity is a saddle of the map ϕ. At $p = 0$ the crossing map at the singularity can exhibit an elliptic sector (a region within which every orbit converges on the singularity both forward and backward in time).

(c3) For $p < 0$ the singularity is a center of the map ϕ. For $p > 0$ a focus cycle emerges from the singularity, and the singularity is a saddle of the map ϕ.

Caution must be taken in studying the dynamics of the system (2.1), since the map (3.12) applies only on the domain $D \subset \mathrm{CR}_1$ (described above (3.9)), from which orbits return to CR_1. Finally, some issues remain unaddressed regarding the invariant sets and the structural stability of crossing dynamics. The bifurcations that must occur at the transition between scenarios (c1) and (c3), for p near 0 suggest the existence of other structures, e.g., quasiperiodic orbits, that may emerge as p crosses 0. Also, as we have seen, when $p < 0$ the map (3.9) is a (nonlinear) rotation from ES to SL. A structurally unstable scenario occurs when the image of the border of ES under ϕ (or multiple iterations of ϕ) is tangent to the border of SL. This is associated with a change in the number of iterations it takes to map points from the border of ES into SL. This issue is the subject of ongoing study.

3.3. Reassembling the Teixeira singularity. Once the dynamics of both the sliding, the escaping, and the crossing regions have been decoded, they can be stitched together to obtain the overall portrait of orbits around the singularity. The dynamics in SL is completely described in section 3.1 and can be of only two types, (s1) and (s2) in Figure 5, depending on the sign of parameter a_2 in (3.7). The dynamics in CR_1 and CR_2 is derived directly from the map (3.12). The changes of variables that place the generic Poincaré map (3.9) in the form (3.12) ensures that, for p sufficiently close to 0, the positive u_1 axis lies strictly inside the domain D of the map ϕ. Hence both the origin and the negative solution of (3.14) are fixed points of the Poincaré map. In particular, in terms of the dynamics of system (2.1), the origin is a limit point (backward or forward in time) of crossing orbits, while the solution (3.14) corresponds to a crossing cycle whose type (focus/node/saddle, stable/unstable) depends, as we have seen in section 3.2, on the coefficients B_{30} and B_{11} of the normal form.

Combining all of these considerations, we can sketch the crossing orbits of system (2.1) (or rather of their intersections with the switching manifold) as in Figure 5, cases (c1)–(c3). The depicted phase portraits are obtained by taking the dynamics of map (3.12), restricted to CR_1, and reflected in the line $x_1 = x_2$. In cases (c2) and (c3) Figures 5 the map contains a node or focus, which can be either stable ((c2$_s$) and (c3$_s$)) or unstable ((c2$_u$) and (c3$_u$)). The complete dynamics around the Teixeira singularity is obtained by stitching together any one of the portraits (s1), (s2) for the sliding dynamics, with any one of the portraits (c1)–(c3) for the crossing dynamics, for a grand total of ten qualitatively different phase portraits.

It should be remarked that, although we derived the crossing dynamics from generic forms for the maps $\phi^{\pm}$ in section 3.2, the crossing dynamics can be derived directly by integrating a local series expansion of the vector fields $f^{\pm}$, allowing them to be compared directly to the sliding vector field f^s. From the (lengthy) expressions obtained for $\phi^{\pm}$, no conditions have been found that prohibit any of the ten possible combinations of sliding portraits (s1), (s2), with crossing portraits (c1)–(c3). Indeed, in Table 7.1 of section 7 we give examples that exhibit each one of the ten possible portraits.

A number of interesting qualitative features of the dynamics can now be directly inferred from Figure 5. For $p < 0$, the crossing dynamics near the singularity is similar in each case (c1)–(c3), in that a finite number of crossings take orbits from ES to SL. Once they reach SL, the vector fields in (s1)–(s2) come into effect, and for $p < 0$ these show that all orbits evolve

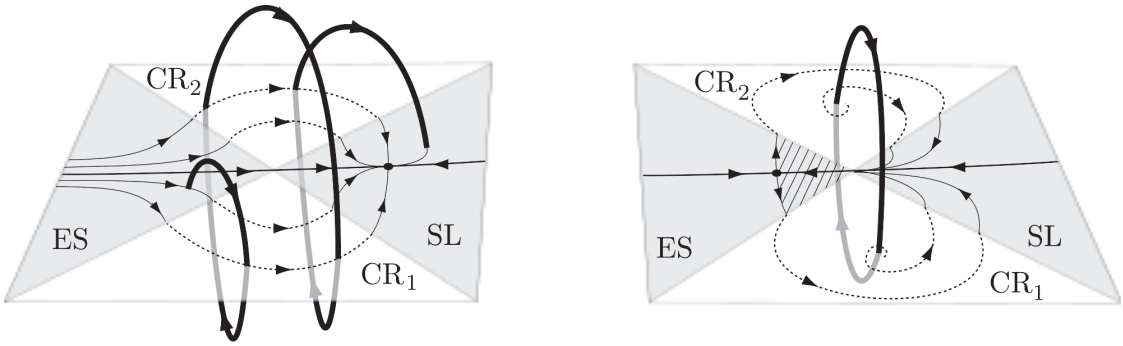

Figure 6. *Composite of the sliding portrait* (s1) *and the crossing portrait* ($c3_u$) *in Figure 5. For $p < 0$ all orbits reach the sliding region, and a crossing orbit is illustrated. For $p > 0$ this system has an invariant set near the singularity, generated by the forward evolution of the hatched region in ES. The limit cycle (fixed point of the map ϕ) is shown.*

away from the singularity, either converging toward a pseudonode in (s1), or leaving the local neighborhood in (s2).

For $p > 0$, however, (c1) is fundamentally different from (c2) and (c3). In (c1), crossing orbits leave the neighborhood of the singularity in either forward or backward time, and importantly, no crossing orbits exist locally that pass from ES to SL. In (c2) and (c3), there always exist crossing orbits that can locally pass from ES to SL. The crossing map contains a fixed point of node or focus type. If the fixed point is stable (($c2_s$) or ($c3_s$)), then all crossing orbits that emerge from ES sufficiently close to the singularity converge toward the fixed point. If the fixed point is unstable (($c2_u$) or ($c3_u$)), then all crossing orbits sufficiently close to the singularity will reach SL in finite time.

Clearly $p > 0$ produces richer crossing dynamics than $p < 0$, but when the associated sliding dynamics is taken into account, the full implications of the Teixeira singularity become apparent. In (s1) and (s2), for $p > 0$, all sliding orbits sufficiently near the singularity pass from SL to ES. In (s2), sliding orbits asymptotic to the unstable manifold of a pseudosaddle either approach the singularity in finite time or leave the local neighborhood. In (s1), however, all local sliding orbits converge on the singularity in finite time. The path followed by an orbit that enters ES through the singularity is then not uniquely determined, as explained in section 3.1.

3.4. Nondeterministic chaos. A particularly interesting case is revealed if we take the crossing portraits ($c2_u$) or ($c3_u$) and combine them with the sliding portrait (s1), as exemplified in Figure 6 and the following result.

Proposition 3.1. *If a system exhibits a Teixeira singularity with the crossing portraits* ($c2_u$) *or* ($c3_u$) *with $p > 0$, and the sliding portrait* (s1), *then locally*

- *all crossing orbits reach SL, with the exception of the unstable limit cycle,*
- *all sliding orbits reach ES via the singularity, and therefore*
- *all orbits visit the singularity recurrently.*

The forward time evolution from the singularity is set-valued, however, and therefore nondeterministic. We can characterize this behavior by saying that the system exhibits a nondeterministic form of chaos. The term "nondeterministic chaos" has previously appeared in [8] in a somewhat different setting, though referring to a similar loss of uniqueness in which an infinity of orbits recurrently pass through a single point in finite time. To properly define this unfamiliar notion, we can begin from the definition of deterministic chaos available in many standard texts. The definition provided in [23] is as follows.

Definition 3.2. *A flow ψ is chaotic on a compact invariant set X if ψ is transitive and exhibits sensitive dependence on X.*

Indeed, the system described in Proposition 3.1 has an invariant set X near the singularity, generated by the forward evolution of the region in ES enclosed by the folds and the unstable manifold of the pseudosaddle (including the pseudosaddle; see hatched region in Figure 6). To define transitivity and sensitivity to initial conditions, we adapt the definition given in [23] to apply to a set-valued flow. First, as in [23], we say the following.

Definition 3.3. *A flow ψ is topologically transitive on an invariant set X if for every pair of nonempty open sets U and V in X there is a $t > 0$ such that $\psi_t(U) \cap V \neq \emptyset$.*

This is satisfied by the system described in Proposition 3.1 since any point $\mathbf{x} \in U$ reaches the singularity in finite time when its forward evolution generates the whole set X. Then, the definition of sensitivity in [23] is adapted to apply to a set-valued flow as follows.

Definition 3.4. *Let $B_\epsilon(\mathbf{x})$ be a ball of radius ϵ centered on $\mathbf{x}$. A set-valued flow ψ exhibits sensitive dependence on an invariant set X if there is a fixed r such that for each $\mathbf{x} \in X$ and any $\epsilon > 0$ there is a nearby $\mathbf{y} \in B_\epsilon(\mathbf{x}) \cap X$ such that the diameter of $\psi_t(\mathbf{x}) \cup \psi_t(\mathbf{y})$ is greater than r for some $t \geq 0$.*

The only difference between this definition and that in [23] is that it uses the diameter of $\psi_t(\mathbf{x}) \cup \psi_t(\mathbf{y})$ instead of the distance $\|\psi_t(\mathbf{x}) - \psi_t(\mathbf{y})\|$. The two definitions coincide for single-valued flows, making this a natural extension for a set-valued flow. For our set-valued flow, the forward evolution of any point in X generates the whole invariant set after crossing the singularity, the flow in Proposition 3.1 exhibits sensitive dependence on initial conditions, and X is a nondeterministic chaotic set.

In section 7 we simulate a system exhibiting nondeterministic chaos and provide examples of systems exhibiting of all other types of Teixeira singularity. Now, for completeness, we turn to the description of the other possible types of two-fold.

4. The visible two-fold. A vector field with transversely intersecting visible folds generically satisfies (2.5)–(2.7), with $\mathcal{L}^2_{f^-} h < 0 < \mathcal{L}^2_{f^+} h$ at their intersection, which is then a visible two-fold. This is illustrated in Figure 7(i) and has the local form

$$f^+ = \begin{pmatrix} -x_1 + \mathcal{O}(x_0, \|x_1, x_2\|^2) \\ -1 \ + \mathcal{O}(\|\mathbf{x}\|) \\ -V^+ + \mathcal{O}(\|\mathbf{x}\|) \end{pmatrix}, \tag{4.1a}$$

$$f^- = \begin{pmatrix} x_2 + \mathcal{O}(x_0, \|x_1, x_2\|^2) \\ -V^- + \mathcal{O}(\|\mathbf{x}\|) \\ -1 \ + \mathcal{O}(\|\mathbf{x}\|) \end{pmatrix}. \tag{4.1b}$$

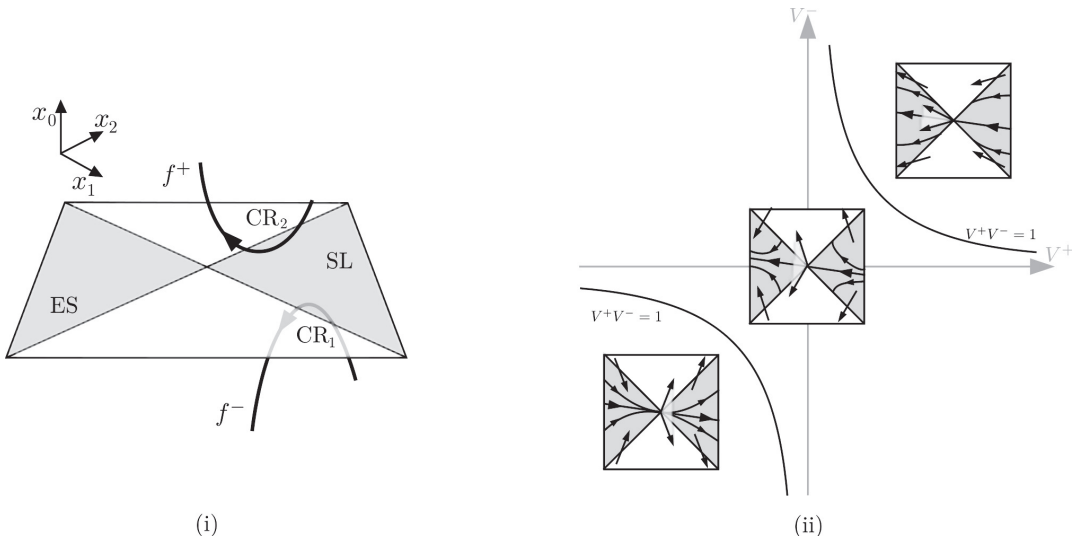

Figure 7. *Dynamics near a visible two-fold:* (i) *orbits outside the switching manifold curve away from the folds,* (ii) *phase portraits of the sliding dynamics. At the origin the sliding vector field f^s is set-valued, with elements pointing into the sliding region SL when $V^+V^- > 1$ and $V^+, V^- < 0$. In this case a one-parameter family of orbits intersects the origin along a unique direction (an eigenvector of the regularization $\tilde{f}^s$ of f^s). In all other cases the set-valued f^s has elements which point into SL and only a single orbit that intersects the singularity.*

The parameters V^+ and V^- can be retrieved for a general vector field at a visible two-fold as

$$V^+ = \frac{-\mathcal{L}_{f^+}\mathcal{L}_{f^-}h}{\sqrt{-(\mathcal{L}^2_{f^+}h)(\mathcal{L}^2_{f^-}h)}}, \tag{4.2a}$$

$$V^- = \frac{\mathcal{L}_{f^-}\mathcal{L}_{f^+}h}{\sqrt{-(\mathcal{L}^2_{f^+}h)(\mathcal{L}^2_{f^-}h)}}. \tag{4.2b}$$

Crossing dynamics in this case are trivial, since all crossing orbits leave the neighborhood of the singularity (see Figure 7(i)). Sliding dynamics can be understood by the same means as in section 3.2. In this case, the equilibrium at the origin in the regularized vector field $\tilde{f}^s$ has eigenvalues

$$\mu_\pm = -\frac{1}{2}\left(V^+ + V^- \pm \sqrt{(V^+ - V^-)^2 + 4}\right) \tag{4.3}$$

(the negative of (3.5)), while the associated eigenvectors are

$$\begin{pmatrix} \mu_\pm + V^+ \\ -1 \end{pmatrix} \tag{4.4}$$

(the same as (3.6)). Thus, sliding dynamics is the same as at the Teixeira singularity (invisible two-fold), but with time-reversed (Figure 7(ii)). This time-reversal has an important

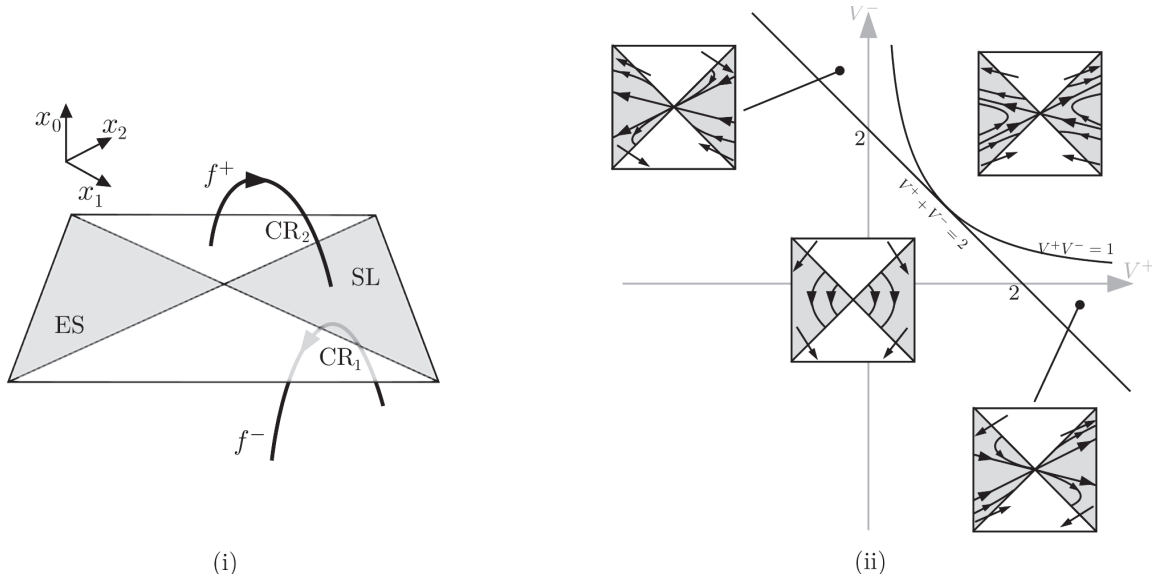

Figure 8. *Dynamics near a visible-invisible two-fold:* (i) *orbits outside the switching manifold curve away from the manifold at one fold and toward it at the other;* (ii) *phase portraits of the sliding dynamics. The singularity in each of SL and ES is intersected by two orbits if* $V^+V^- > 1$ *and* $V^+, V^- > 0$*, a one-parameter family of orbits if* $V^+V^- < 1$ *and* $V^+ + V^- > 2$*, and no orbits otherwise. As in previous cases, the orbits intersect the singularity along the eigenvectors of* $\tilde{f}^s$ *(the regularization of* f^s*), and the sliding vector field* f^s *is set-valued (not shown) at the singularity.*

implication for the complexity of the local dynamics. Similarly to the Teixeira singularity, a pseudoequilibrium crosses between SL and ES when $V^+V^- = 1$ with $V^+, V^- < 0$. However, whereas at a Teixeira singularity a one-parameter family of orbits in SL can intersect the singularity, at a visible two-fold only a single orbit in SL can intersect the singularity. In any event, all trajectories evolve away from the singularity into the upper or lower vector fields, leaving the switching manifold either from a visible fold or from ES. As shown in [14], the portraits in Figure 7(ii) are all the structurally stable cases near the singularity.

5. The visible-invisible two-fold. A vector field with transversely intersecting visible and invisible folds generically satisfies (2.5)–(2.7), with $(\mathcal{L}^2_{f^-}h)(\mathcal{L}^2_{f^+}h) > 0$ at the singularity, which is then a visible-invisible two-fold. This is illustrated in Figure 8(i) and has the local form

$$f^+ = \begin{pmatrix} -x_1 + \mathcal{O}(x_0, \|x_1, x_2\|^2) \\ 1 + \mathcal{O}(\|\mathbf{x}\|) \\ V^+ + \mathcal{O}(\|\mathbf{x}\|) \end{pmatrix}, \tag{5.1a}$$

$$f^- = \begin{pmatrix} x_2 + \mathcal{O}(x_0, \|x_1, x_2\|^2) \\ -V^- + \mathcal{O}(\|\mathbf{x}\|) \\ -1 + \mathcal{O}(\|\mathbf{x}\|) \end{pmatrix}. \tag{5.1b}$$

The parameters V^+ and V^- can be retrieved for a general vector field at a visible-invisible two-fold as

$$V^+ = \frac{\mathcal{L}_{f^+}\mathcal{L}_{f^-}h}{\sqrt{(\mathcal{L}^2_{f^+}h)(\mathcal{L}^2_{f^-}h)}}, \tag{5.2a}$$

$$V^- = \frac{\mathcal{L}_{f^-}\mathcal{L}_{f^+}h}{\sqrt{(\mathcal{L}^2_{f^+}h)(\mathcal{L}^2_{f^-}h)}} \tag{5.2b}$$

(note that for this case there is no "−" sign inside the square root). The presence of a visible fold prevents the onset of recurring crossing dynamics around the singularity. Concerning sliding dynamics (Figure 8(ii)), the equilibrium at the origin of the regularized vector field $\tilde{f}^s$ has eigenvalues

$$\mu_\pm = \frac{1}{2}\left(V^+ - V^- \pm \sqrt{(V^+ + V^-)^2 - 4}\right), \tag{5.3}$$

while the associated eigenvectors are

$$\begin{pmatrix} \mu_\pm - V^+ \\ -1 \end{pmatrix}. \tag{5.4}$$

The eigenvalues are imaginary when $|V^+ + V^-| < 2$ and real otherwise. When $V^+ + V^- < 2$, regardless of whether $V^+V^- > 1$ or $V^+V^- < 1$ (in the former case $\tilde{f}^s$ has a saddle, in the latter $\tilde{f}^s$ has a focus), orbits flow around the singularity, entering SL and ES from one fold and exiting from the other. Less trivial dynamics appears when $V^+ + V^- > 2$. The eigenvalues are real, and both eigenvectors point toward SL or ES. When $V^+V^- = 1$, an eigenvalue goes to 0. In this case $\tilde{f}^s$ has a one-dimensional center manifold (see Appendix E) with dynamics

$$\dot{u} = (V^+V^- - 1)u + a_2u^2 + \mathcal{O}(u^3). \tag{5.5}$$

As V^+V^- passes through unity with $V^+, V^- > 0$, a pseudoequilibrium crosses the singularity along the singular eigenvector. The structural stability of the orbits in Figure 3 depends on the composition of the sliding/escaping portraits with the map ϕ^+. As shown in [14], this subdivides Figure 3(ii) into 11 regions of structurally different dynamics, depending on the sequences of escaping-crossing-sliding that families of orbits can undergo. As a final remark, inspection of the wedge $V^+V^- < 1$, $V^+ + V^- > 2$, $V^- > V^+$ in Figure 3(ii) may suggest the possibility of nondeterministic chaos if ϕ^+ maps escaping orbits emerging from the singularity to sliding orbits entering the singularity. A short calculation from (5.1), however, shows that, locally, the direction of ϕ^+ does not allow this.

6. A remark on sliding bifurcations and invariant manifolds. Although the local behavior of the visible and visible-invisible two-folds is less complex than that of the Teixeira singularity, it can have striking implications for global dynamics. First, we see in Figures 7 and 8 that orbits do exist crossing the two-fold from the sliding to escaping regions. This is locally less

interesting because all orbits eventually depart the neighborhood of the two-fold, leaving the switching manifold via a visible fold. This same reasoning, however, means that the local sliding dynamics will interact with the global dynamics. It is then known that one-parameter families of orbits can undergo so-called catastrophic sliding bifurcations, introduced in [17]. In these bifurcations, for example, periodic orbits can be suddenly destroyed through encounter with a visible or visible-invisible two-fold. This occurs when they cross the two-fold from SL to ES, so the local geometry is provided by the vector fields in sections 4–5. In some cases, for example in Figure 8 with $V^+V^- < 1$, $V^+ + V^- > 2$, $V^+ < V^-$, these bifurcations are likely to be associated with nondeterministic chaotic dynamics on a global scale. Also, codimension-one invariant manifolds in n-dimensional systems can generically contain visible or visible-invisible two-folds where they intersect a switching manifold, and the three-dimensional case was discussed in [7]. Again, their local behavior is provided by the analysis above.

7. Numerical simulations. The lowest order approximation to the Teixeira singularity analyzed in [16] revealed an interesting bifurcation, in the form of an invariant nonsmooth diabolo (an invariant double cone with a crease at the switching manifold) that self-annihilates through a loss of hyperbolicity. The higher order analysis in this paper fully unveils this bifurcation's intriguing nonlinear behavior, depicted in Figure 5. A compellingly peculiar case, as we have seen in section 3.3, is obtained by combining the sliding portrait from Figure 5(s1) with the crossing portrait from Figure 5(c3$_u$), obtained by taking (2.4) and (3.9) with coefficients $B_{11} > 0$, $B_{30} < 0$, $|8B_{30}| > B_{11}^2$, and $a_2 > 0$, as $p = V^+V^- - 1$ changes sign. When $p > 0$, this scenario exhibits a nondeterministic chaotic set: the sliding dynamics channels orbits from SL to ES, with all information on initial data lost at the singularity, while the crossing dynamics provides a mechanism for reinjection to SL. Thus the local neighborhood is recurrently visited by orbits ejected from the singularity, and their history is lost with each visit. Orbits are unique in neither forward nor backward time, but, by varying a parameter through the nonsmooth diabolo bifurcation, the system can be controlled toward the benign case ($p < 0$). A numerical example of this case is provided by the following system:

$$f^+ = \begin{pmatrix} -3 & -1 & 0 \\ -1 & -3 & 0 \\ 0 & 1 & -2 \end{pmatrix} \begin{pmatrix} x_0 \\ x_1 \\ x_2 \end{pmatrix} + \begin{pmatrix} 0 \\ 1 \\ V^+ \end{pmatrix}, \tag{7.1a}$$

$$f^- = \begin{pmatrix} 3 & 0 & 1 \\ 0 & -2 & 0 \\ 1 & 0 & 3 \end{pmatrix} \begin{pmatrix} x_0 \\ x_1 \\ x_2 \end{pmatrix} + \begin{pmatrix} 0 \\ V^- \\ 1 \end{pmatrix}, \tag{7.1b}$$

with a switching manifold $x_0 = 0$. The sliding and crossing normal forms (3.7) and (3.12) at the nonsmooth diabolo bifurcation for this system have coefficients $B_{11} = -16$, $B_{30} = -1662.93$, $a_2 = 61.4$, when $V^+ = -5$ and $V^- = -1/5$, thus falling into case (s1)-(c3$_u$) of the Teixeira singularity. In Figure 9, we have simulated the system using the software MATLAB, with a piecewise smooth numerical integrator [27] for $V^+ = -5.01$ and $V^- = -1/5$, thus $p = V^+V^- - 1 = 0.002$. Because we are close to the bifurcation ($|V^+V^- - 1| \ll 1$ with $V^+, V^- < 0$), the vector fields above and below the switching manifold are almost antiparallel at the origin. This causes strong squashing of orbits toward a plane transverse to the switching manifold, observable in Figure 9(i) and also seen from the crossing points in Figure 9(ii). Here

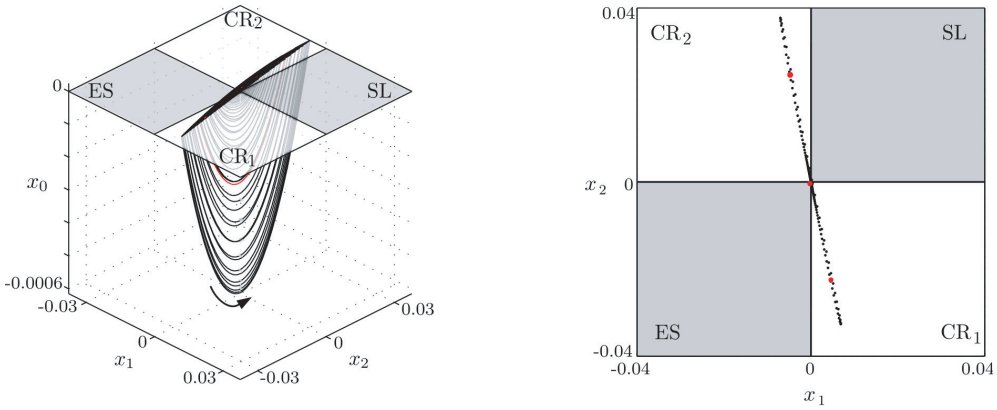

(i) (ii)

Figure 9. *Simulation of system (7.1) with $V^+ = -5.01$ and $V^- = -1/5$, exhibiting a pseudoequilibrium in ES and an unstable focus cycle.* (i) *A single orbit originating near ES, with initial conditions $(10^{-20}, -10^{-6}, -10^{-6})$, winds around the singularity and reaches SL, then is attracted toward the singularity and back into ES.* (ii) *Intersections of the orbit with the switching manifold. The pseudoequilibrium in ES and the crossing points of the focus cycle are highlighted in bold.*

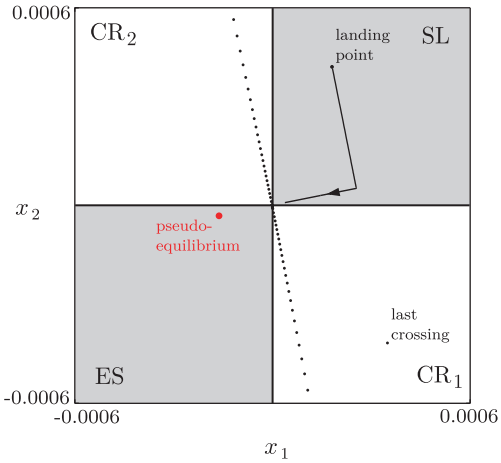

Figure 10. *Magnification of Figure 9(ii) near the origin. As the orbit departs from its initial condition near the singularity, its crossing points lie (approximately) along a line through the origin, and the orbit's last crossing point lies in the lower right corner of CR_1. The orbit's entry point into SL is seen, followed by its sliding trajectory towards the singularity. A pseudoequilibrium is shown in ES (red dot).*

the dynamics in the direction transverse to this plane cannot be resolved; in particular, the orbit's evolution in SL cannot be seen. We resolve the orbits in the following two figures.

Figure 10 presents a simple magnification of the Poincaré map from Figure 9(ii) around the singularity. The line of points emanating from the origin are the crossing points of the orbit as it leaves the neighborhood of the singularity. After the last crossing (lower right corner of CR_1), the orbit is seen to impact SL toward the top of the figure, evolve via an almost straight path toward the point $(x_1, x_2) \simeq (0.00025, 0.00005)$, then to the singularity.

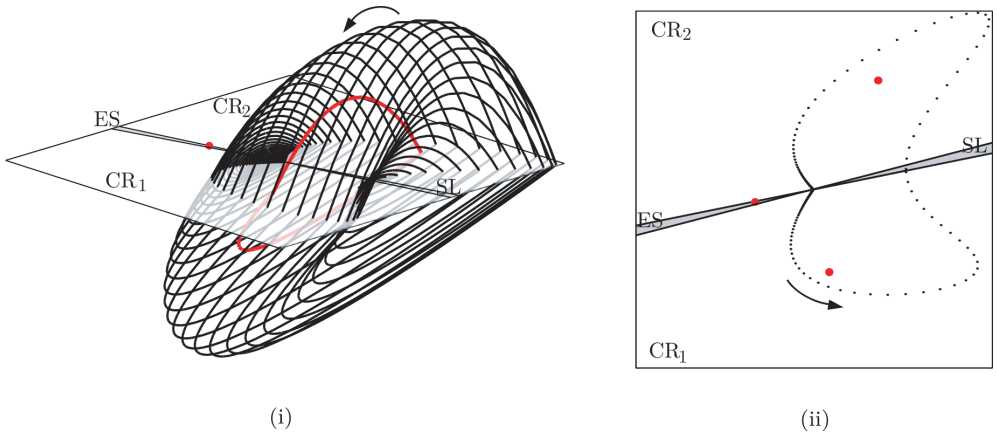

Figure 11. *A magnification of Figure 9, making a linear coordinate change in the x_1-x_2 plane and stretching the positive x_0 axis by a factor of 20. In* (i) *the orbit can now be seen, crossing repeatedly through the switching manifold and surrounding the focus cycle (depicted in red). In* (ii), *the orbit's crossing points are seen to form a butterfly shape around the two (red) crossing points of the focus cycle.*

From the simulation we confirm that the orbit reaches the singularity in time $t \simeq 0.48$ after reaching SL. At this time the integrator fails to work, since the orbit is entering ES where its evolution becomes non-unique.

Figure 11 presents the orbits in Figure 9 under a linear coordinate change in the x_1-x_2, plane. We have also stretched the coordinate x_0 by a factor of 20 above the switching manifold only. A single orbit is shown, whose initial point is at $(10^{-20}, -10^{-6}, -10^{-6})$, which lies a small distance from the singularity and above ES. The orbit winds around the singularity a large number of times and eventually maps into the interior of SL, from where it is inevitably pulled into the singularity as shown in Figure 10. This is consistent with the phase portraits predicted in case (s1)-(c3) and illustrated in Figure 6. Upon reaching the singularity, the system can follow any one of an infinite number of trajectories, independent of the orbit's history. This therefore demonstrates that the predicted conditions for nondeterministic chaos exist. We now show that this behavior can be tamed by varying the parameter p. We change V^+ to the value -4.99, for which $p = V^+V^- - 1 = -0.002$. This system is simulated in Figure 12(i), with a rescaling in (ii) (the same scaling as in Figure 11(ii)) to resolve the fine structure of the orbits. A single orbit is shown and has the same initial condition as in Figure 9. The orbit winds around the singularity a large number of times and reaches SL. In this case the sliding orbit is repelled from the singularity along a visibly straight path, as can be seen in Figure 12(i). The orbit terminates at a pseudoequilibrium, which can be seen at the edge of SL.

It is easy to confirm (as reported in [16, 17]) that trajectories of the truncated leading order system in (3.1) are curves $(x_0(t), x_1(t), x_2(t))$ whose coordinates satisfy

$$(V^+V^- - 1)|x_0| = \begin{cases} \left(\dfrac{1}{2V^-}x_1^2 + \dfrac{1}{2V^+}x_2^2 - x_1x_2 + c\right)V^- & \text{if } x_0 > 0, \\ \left(\dfrac{1}{2V^-}x_1^2 + \dfrac{1}{2V^+}x_2^2 - x_1x_2 + c\right)V^+ & \text{if } x_0 < 0, \end{cases} \tag{7.2}$$

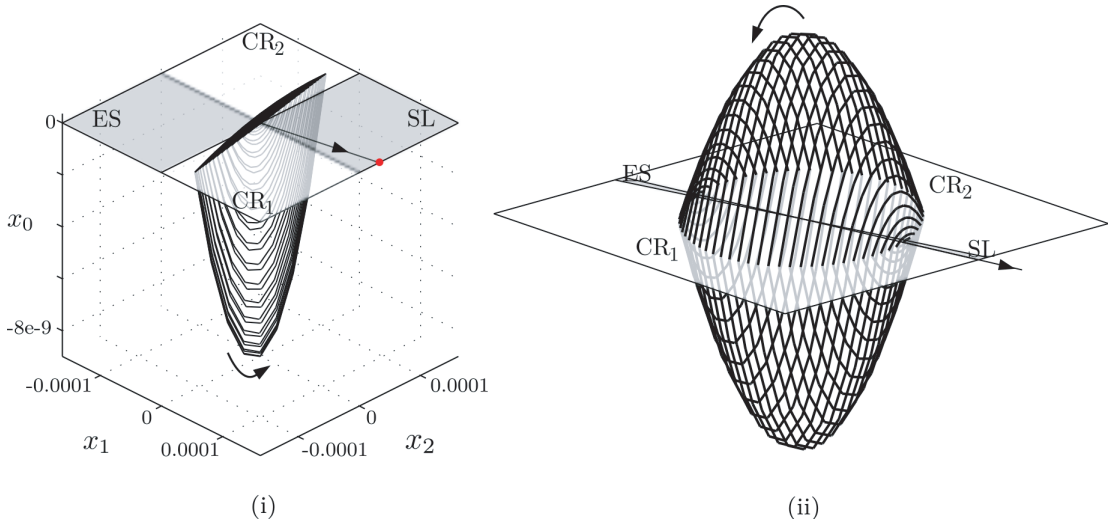

Figure 12. *Simulation of system (7.1) with $V^+ = -4.99$ and $V^- = -1/5$, with a pseudoequilibrium in SL.* (i) *A single orbit originating near ES, with initial conditions $(10^{-20}, -10^{-6}, -10^{-6})$, winds around the singularity and reaches SL, and then is repelled from the singularity toward a pseudoequilibrium (red dot at edge of SL).* (ii) *A linear coordinate change in the x_1-x_2 plane, and a stretching of the positive x_0 axis by a factor of 20, resolves the crossing dynamics of the orbit.*

where the constant c fixes the height that the orbit attains along the x_0 axis. When $V^+V^-(1-V^+V^-) > 0$, these equations define a pair of paraboloids, one above and one below the switching manifold, joined nondifferentiably, forming a ball with a creased equator. When $V^+V^-(1-V^+V^-) < 0$, they similarly define a pair of surfaces above and below the switching manifold, each of which is part of a saddle, again joined nondifferentiably. In Figure 12(ii), the two adjoined paraboloids are clearly seen. In Figure 11(i) higher order terms govern the behavior of the trajectories away from the singularity, but near the singularity they can be seen to lie on portions of saddles. If $c = 0$, the surfaces form a nonsmooth double cone—a diabolo—through the singularity, which undergoes the nonsmooth diabolo bifurcation when $p = 0$ [16].

Finally, for the reader's interest, we provide examples of systems exhibiting each of the ten different portraits in Figure 5. We consider system (7.1), changing the Jacobian of f^+ to

$$\begin{pmatrix} a_{11} & -1 & 0 \\ -1 & -3 & 0 \\ 0 & a_{32} & -2 \end{pmatrix}. \tag{7.3}$$

By assigning the values in Table 7.1 to the parameters a_{11}, a_{32}, V^+, and V^-, we obtain an example of each predicted scenario. It is a simple exercise to recast (7.3) in the form of a relay system (see, e.g., [31]), implying that it might easily arise in electrical or control applications. It is conceivable that the singularity occurs in various piecewise smooth dynamical systems where the generic conditions (2.5)–(2.7) are satisfied.

Table 7.1

List of parameter values a_{11}, a_{32}, V^+, and V^- used to obtain examples of all portraits depicted in Figure 5, using the system (7.1) with the Jacobian of f^+ modified as in (7.3).

Portrait	a_{11}	a_{32}	V^+	V^-
s1-c1	-3	1	$-1/20$	-20
s1-c2$_s$	-3	1	$-1/5$	-5
s1-c2$_u$	100	0	-20	$-1/20$
s1-c3$_s$	-3	1	-1	-1
s1-c3$_u$	-3	1	-5	$-1/5$
s2-c1	-3	10	$-1/2$	-2
s2-c2$_s$	-3	10	$-2/3$	$-3/2$
s2-c2$_u$	100	100	-5	$-1/5$
s2-c3$_s$	-3	10	-1	-1
s2-c3$_u$	-3	100	-5	$-1/5$

8. Conclusions. We have reviewed the local description of the singularity formed when a three-dimensional piecewise smooth vector field is tangent to both sides of a switching manifold—a two-fold singularity. We analyzed the dynamics of orbits in regions of sliding, identifying conditions that cause a pseudoequilibrium to pass through the singularity. This represents a novel bifurcation through which a pseudoequilibrium can collide with a boundary of a sliding or escaping region, fundamentally different from the well-known boundary equilibrium bifurcations in Filippov systems [10]. We conclude that, in some cases, families of sliding orbits are attracted to the singularity, making the intersection of an orbit with a two-fold a generic event. This allows solutions starting away from the escaping region to reach it. These facts are often overlooked in the literature (see, e.g., [10, 11, 27]). We also analyzed the dynamics of crossing orbits, concluding that if one of the folds is visible (local trajectories curve away from the switching manifold along it), then all orbits eventually leave the neighborhood of the singularity. These cases, (sections 4–5), are of interest when they interact with other attractors or invariant sets outside the neighborhood of the two-fold. The case that is most dynamically interesting in its own right is the Teixeira singularity.

The Teixeira singularity consists of two invisible folds, which cause all local trajectories to curve toward the manifold. This case exhibits a number of local bifurcations, which we unfolded by separately analyzing the bifurcation of the smooth systems that describe the local crossing and sliding dynamics. The crossing dynamics is described by a return map that undergoes a degenerate 1:1 resonance bifurcation. This coincides with the passage of a pseudoequilibrium through the singularity, from SL to ES or vice versa. One parameter, the quantity V^+V^-, characterizes the leading order problem and measures the angular disparity between the vector fields above and below the switching manifold, evaluated at the origin. A normal form reduction of the neighboring dynamics reveals that the qualitative behavior of a local unfolding depends on three coefficients, two characterizing the stability and topological type of the fixed points of the crossing map, and one the position of the pseudoequilibrium. The unfolding reveals the bifurcation of the Teixeira singularity as a new route to the sudden appearance of periodic orbits and more complex invariant sets in piecewise smooth systems.

Among the local dynamics possible near a Teixeira singularity, we have identified one that is particularly intriguing. It occurs when, for a whole family of parameters where $V^+V^- > 1$ with $V^+, V^- < 0$, the crossing map contains an unstable focus (an unstable limit cycle of the full system) and the pseudoequilibrium is a saddle. Here we find conditions for nondeterministic chaos over a compact neighborhood of the singularity. All local orbits begin and end at the singularity, with a definite direction through it, but on each visit their history is lost and their forward evolution is nonunique. We have simulated an example of this scenario in section 7, depicting one such orbit in Figures 9, 10, and 11. We verified in numerical simulations that the conditions for this recurrent nondeterministic dynamics exist, but the phenomenon can be tamed by changing the parameters V^+ and V^-, through a nonsmooth diabolo bifurcation [16]. After the bifurcation, orbits wrap around a nonsmooth ball, going from ES to SL. Once in SL, they evolve away from the singularity, so that in this case a typical orbit never encounters the singularity.

By stripping the two-fold down to the leading order behavior of its sliding and crossing dynamics, we have unfolded its bifurcations and unveiled its determinacy-destroying heart. But we cannot yet claim that this troublesome singularity is fully understood. The bifurcation diagram of the crossing return map in Figure 5 is incomplete: global bifurcations, yet unknown, occur between the identified scenarios or each time the invariant manifolds of the crossing map, or the images of the boundaries of ES, become tangent to the folds. Much grander challenges than this remain, however. In systems of dimension $n \geq 4$ the two-fold generically has dimension $n-3$. How much of the local dynamics revealed in this paper will survive in higher dimensions remains to be studied. Moreover, even in three dimensions any of the three flavors of two-folds can interact with nonlocal attractors, causing global bifurcations that have not been considered to date.

Appendix A. Normal form reduction of the sliding vector field of a Teixeira singularity. The normal form (3.7) is obtained by multiplying (3.4) by the quantity $(V^+ + 1/V^+)$ and then taking the dynamics along the direction $(-V^+, 1)$ of the singular eigenvector, by defining $\mathbf{x} = \mathbf{p}u$ and $\dot{u} = \mathbf{q}\tilde{f}^s(\mathbf{p}u)$, with $\mathbf{p}$ and $\mathbf{q}$ respectively the right and left singular eigenvectors of the Jacobian of $\tilde{f}^s$ at the origin, when $V^+V^- = 1$ and $V^+, V^- < 0$. Calling c^+_{ij} and c^-_{ij}, for $i, j \in \{1, \ldots, 3\}$, the coefficients of the Jacobians of f^+ and f^-, from this transformation we obtain $\dot{u} = (V^+V^- - 1)u + a_2u^2 + \mathcal{O}(u^3)$, with

$$a_2 = c^+_{22}V^+ - c^+_{23} - c^+_{32} + \frac{c^+_{33}}{V^+} - c^-_{22}(V^+)^2 + c^-_{23}V^+ + c^-_{32}V^+ - c^-_{33}. \tag{A.1}$$

Appendix B. Generic perturbation of the map. Assuming analyticity of the return maps, ϕ^+ can be expanded around the singularity, yielding

$$\begin{aligned} x_1 \mapsto\ & -x_1 + \alpha_{20}x_1^2 + \alpha_{11}x_1x_2 + \alpha_{02}x_2^2 + \alpha_{30}x_1^3 + \alpha_{21}x_1^2x_2 + \alpha_{12}x_1x_2^2 + \alpha_{03}x_2^3 \\ & + \mathcal{O}(\|(x_1, x_2)\|^4), \\ x_2 \mapsto\ & x_2 - 2V^+x_1 + \beta_{20}x_1^2 + \beta_{11}x_1x_2 + \beta_{02}x_2^2 + \beta_{30}x_1^3 + \beta_{21}x_1^2x_2 + \beta_{12}x_1x_2^2 + \beta_{03}x_2^3 \\ & + \mathcal{O}(\|(x_1, x_2)\|^4), \end{aligned}$$

while ϕ^- is equal to

$$\begin{aligned}
x_1 \mapsto\ & x_1 - 2V^- x_2 + \gamma_{20}x_1^2 + \gamma_{11}x_1x_2 + \gamma_{02}x_2^2 + \gamma_{30}x_1^3 + \gamma_{21}x_1^2x_2 + \gamma_{12}x_1x_2^2 + \gamma_{03}x_2^3 \\
& + \mathcal{O}(\|(x_1,x_2)\|^4), \\
x_2 \mapsto\ & -x_2 + \delta_{20}x_1^2 + \delta_{11}x_1x_2 + \delta_{02}x_2^2 + \delta_{30}x_1^3 + \delta_{21}x_1^2x_2 + \delta_{12}x_1x_2^2 + \delta_{03}x_2^3 \\
& + \mathcal{O}(\|(x_1,x_2)\|^4).
\end{aligned}$$

However, the possible values of the maps' coefficients are constrained, since the two maps are involutions and the inducing flow is quadratically tangent to the x_2 and x_1 axes. Imposing that $\phi^+ \circ \phi^+$ and $\phi^- \circ \phi^-$, truncated to third order, be the identity (involution condition), and that ϕ^+ and ϕ^- preserve the x_2 and x_1 axis, respectively, reduces the number of independent coefficients of each map from 15 to 6, yielding

$$\begin{aligned}
x_1 \mapsto\ & -x_1 + \alpha_{20}x_1^2 + \alpha_{21}x_1^2x_2 - (\alpha_{20}^2 + \alpha_{21}V^+)x_1^3 + \mathcal{O}(\|(x_1,x_2)\|^4), \\
x_2 \mapsto\ & x_2 - 2V^+x_1 + \beta_{11}x_1x_2 + (\alpha_{20} - \beta_{11})V^+x_1^2 + \beta_{12}x_1x_2^2 \\
& + \left(\frac{1}{2}\left(-\alpha_{20}\beta_{11} + \beta_{11}^2\right) + (\alpha_{21} - 2\beta_{12})V^+\right)x_1^2x_2 + \beta_{30}x_1^3 + \mathcal{O}(\|(x_1,x_2)\|^4)
\end{aligned}$$

for ϕ^+ and

$$\begin{aligned}
x_1 \mapsto\ & x_1 - 2V^-x_2 + \gamma_{11}x_1x_2 + (\delta_{02} - \gamma_{11})V^-x_2^2 + \gamma_{21}x_1^2x_2 \\
& + \left(\frac{1}{2}\left(-\delta_{02}\gamma_{11} + \gamma_{11}^2\right) + (\delta_{12} - 2\gamma_{21})V^-\right)x_1x_2^2 + \gamma_{03}x_2^3 + \mathcal{O}(\|(x_1,x_2)\|^4), \\
x_2 \mapsto\ & -x_2 + \delta_{02}x_2^2 + \delta_{12}x_1x_2^2 - (\delta_{02}^2 + \delta_{12}V^-)x_2^3 + \mathcal{O}(\|(x_1,x_2)\|^4)
\end{aligned}$$

for ϕ^-. Finally, composing $\phi^- \circ \phi^+$, we obtain the general third order expansion of the Poincaré map ϕ:

$$\begin{aligned}
x_1 \mapsto\ & -x_1 + 2V^-x_2 + a_{20}x_1^2 + a_{11}x_1x_2 + a_{02}x_2^2 + a_{30}x_1^3 + a_{21}x_1^2x_2 + a_{12}x_1x_2^2 + a_{03}x_2^3 \\
& + \mathcal{O}(\|(x_1,x_2)\|^4), \\
x_2 \mapsto\ & -2V^+x_1 + (-1 + 4V^+V^-)x_2 + b_{20}x_1^2 + b_{11}x_1x_2 + b_{02}x_2^2 + b_{30}x_1^3 + b_{21}x_1^2x_2 \\
& + b_{12}x_1x_2^2 + b_{03}x_2^3 + \mathcal{O}(\|(x_1,x_2)\|^4),
\end{aligned}$$

with

$$
\begin{aligned}
a_{20} &= \alpha_{20},\\
a_{11} &= -\gamma_{11} - 4\alpha_{20}V^-,\\
a_{02} &= V^-(-\delta_{02} + \gamma_{11} + 4\alpha_{20}V^-),\\
a_{30} &= -\alpha_{20}^2 - \alpha_{21}V^+,\\
a_{21} &= 2\alpha_{20}\gamma_{11} - \gamma_{21} + 6\alpha_{20}^2V^- + \alpha_{21}(-1 + 6V^-V^+),\\
a_{12} &= \frac{-\gamma_{11}^2}{2} - 6\alpha_{20}\gamma_{11}V^- + \frac{\delta_{02}}{2}(\gamma_{11} + 4\alpha_{20}V^-),\\
&\quad - V^-(-4\alpha_{21} + \delta_{12} - 2\gamma_{21} + 12\alpha_{20}^2V^- + 12\alpha_{21}V^-V^+),\\
a_{03} &= -\gamma_{03} + 4(V^-)^2(\alpha_{20}(-\delta_{02} + \gamma_{11} + 2\alpha_{20}V^-) + \alpha_{21}(-1 + 2V^-V^+))\\
b_{20} &= (-\beta_{11} + \alpha_{20})V^+,\\
b_{11} &= -2(\gamma_{11} + 2\alpha_{20}V^-)V^+ + \beta_{11}(-1 + 4V^+V^-),\\
b_{02} &= \delta_{02} - 2\delta_{02}V^+V^- + 2V^-(\beta_{11} - 2\beta_{11}V^+V^- + (\gamma_{11} + 2\alpha_{20}V^-)V^+),\\
b_{30} &= \beta_{30},\\
b_{21} &= \frac{-\beta_{11}^2}{2} - 6\beta_{30}V^- - \alpha_{21}V^+ + 2\beta_{12}V^+ - 2\beta_{11}\gamma_{11}V^+ - 2\gamma_{21}V^+ + \frac{\alpha_{20}}{2}(\beta_{11} + 4\gamma_{11}V^+),\\
b_{12} &= \beta_{12} + \delta_{12} + 2\beta_{11}^2V^- + 12\beta_{30}(V^-)^2 + \delta_{02}\gamma_{11}V^+ - \gamma_{11}^2V^+ + 4\alpha_{21}V^-V^+\\
&\quad - 8\beta_{12}V^-V^+ + 2\alpha_{20}\delta_{02}V^-V^+ - 2\delta_{12}V^-V^+ - 6\alpha_{20}\gamma_{11}V^-V^+ + 4\gamma_{21}V^-V^+\\
&\quad + \beta_{11}(\delta_{02} - \gamma_{11} - 2\alpha_{20}V^- - 2\delta_{02}V^-V^+ + 6\gamma_{11}V^-V^+),\\
b_{03} &= -\delta_{02}^2 - 2\beta_{12}V^- - 3\beta_{11}\delta_{02}V^- - \delta_{12}V^- + \beta_{11}\gamma_{11}V^- + 2\alpha_{20}\beta_{11}(V^-)^2\\
&\quad - 2\beta_{11}^2(V^-)^2 - 8\beta_{30}(V^-)^3 - 2\gamma_{03}V^+ - 4\alpha_{21}(V^-)^2V^+ + 8\beta_{12}(V^-)^2V^+\\
&\quad - 4\alpha_{20}\delta_{02}(V^-)^2V^+ + 4\beta_{11}\delta_{02}(V^-)^2V^+ + 4\alpha_{20}\gamma_{11}(V^-)^2V^+ - 4\beta_{11}\gamma_{11}(V^-)^2V^+.
\end{aligned}
$$

Appendix C. Normal form reduction of the Poincaré map. When

$$p := V^+V^- - 1 = 0,$$

the Poincaré map has a fixed point, at the singularity, with a nonsemisimple double one linearization. This can be put into a 1:1 resonance normal form which is symmetric, due to the constraints imposed by the involution assumption (see Appendix B). The normal form reduction of map (3.9) is carried out, following a standard path, as a linear transformation followed by a sequence of near-identity transformations (see [21,25]), eliminating nonresonant terms of different degree iteratively. First, the linear part of the map (3.9) is simplified through the parameter-dependent change of variables

$$\begin{pmatrix} x_1 \\ x_2 \end{pmatrix} = \begin{pmatrix} 2 - 4V^+V^- & 1 \\ -2V^+ & 0 \end{pmatrix} \begin{pmatrix} \xi_1 \\ \xi_2 \end{pmatrix},$$

becoming

$$
\begin{aligned}
\xi_1 &\mapsto \xi_1 + \xi_2,\\
\xi_2 &\mapsto 4p\xi_1 + (1 + 4p)\xi_2.
\end{aligned}
$$

This corresponds to the Jordan form of the linearized system when $p = 0$. In the (x_1, x_2) coordinates and at the bifurcation, the coordinate axis ξ_1 points in the direction of the singular eigenvector $(-1, -V^+)$ of $\phi|_{p=0}$, while the axis ξ_2 points in the x_1 direction; hence the change of variables has turned the plane to align the singular eigenvector with the ξ_1 direction, and in the new variables the ξ_1 axis is strictly inside CR_1 and CR_2. This is an important remark, since the crossing map is defined only for orbits in ES, CR_1, and CR_2.

Next, the second order, near-identity change of variables

$$\begin{aligned}\xi_1 &= c_{20}\mu_1^2,\\ \xi_2 &= d_{20}\mu_1^2 + d_{11}\mu_1\mu_2 s + d_{02}\mu_2^2,\end{aligned}$$

with

$$\begin{aligned}c_{20} &= -\frac{b_{20} + 2b_{02}(V^+)^2 + b_{11}V^+ - a_{20}V^+}{V^+(12p + 16p^2 + 2)},\\ d_{20} &= \frac{16b_{20}p + 4b_{20} + 16b_{20}p^2 + 4b_{02}(V^+)^2 + 4b_{11}V^+ + 2V^+4b_{11}p}{2V^+},\\ d_{11} &= -\frac{6b_{20} + 4b_{02}(V^+)^2 + 4b_{11}V^+ - 2a_{20}V^+ + 32b_{20}p + 80b_{20}p^2}{V^+(12p + 16p^2 + 2)}\\ &\quad + \frac{64b_{20}p^3 + 3V^+4b_{11}p + V^+16b_{11}p^2}{V^+(12p + 16p^2 + 2)},\\ d_{02} &= \frac{-4b_{02}(V^+)^2 - 2b_{11}V^+ + 2a_{20}V^+ + 12b_{20}p + 16b_{20}p^2}{2V^+(12p + 16p^2 + 2)},\end{aligned}$$

simplifies the quadratic terms, giving

$$\begin{aligned}&\mu_1 \mapsto \mu_1 + \mu_2,\\ &\mu_2 \mapsto 4p\mu_1 + (1 + 4p)\mu_2 + B_{20}\mu_1^2 + B_{11}\mu_1\mu_2,\end{aligned}$$

with

$$\begin{aligned}B_{20}|_{p=0} &= 4(a_{20} - b_{11} - b_{20}V^- + a_{11}V^+ - b_{02}V^+ + a_{02}(V^+)^2),\\ B_{11}|_{p=0} &= -4b_{02}V^+ - 2b_{11} - 2a_{11}V^+ - 4a_{20}.\end{aligned}$$

Due to the involution condition, the term $B_{2,0}$ is identically null near $p = 0$, and this second order expansion is structurally unstable. In order to obtain the topological normal form of the Poincaré map, the third order expansion must be considered. Once again, through the near-identity transformation

$$\begin{aligned}\mu_1 &= u_1 + e_{30}u_1^3 + e_{21}u_1^2u_2,\\ \mu_2 &= u_2 + f_{30}u_1^3 + f_{21}u_1^2u_2 + f_{03}u_2^3,\end{aligned}$$

we simplify the terms of degree 3 in the expansion of the map, obtaining the normal form

$$\begin{aligned}&u_1 \mapsto u_1 + u_2 + \mathcal{O}(\|\mathbf{u}\|^4),\\ &u_2 \mapsto 4pu_1 + (1 + 4p)u_2 + B_{11}u_1u_2 + B_{30}u_1^3 + B_{21}u_1^2u_2 + B_{03}u_2^3 + \mathcal{O}(\|\mathbf{u}\|^4).\end{aligned}$$

Appendix D. Approximation by a flow. A flow whose unit-time shift approximates map (3.12) is easily found by means of successive Picard iterations, as explained, e.g., in [20]. For $p = 0$, this is

$$\dot{u}_1 = u_2 - \frac{B_{11}}{2}u_1u_2 + \frac{B_{11}}{3}u_2^2 + C_{30}u_1^3 + C_{21}u_1^2u_2 + C_{12}u_1u_2^2 + C_{03}u_2^3,$$
$$\dot{u}_2 = B_{11}u_1u_2 - \frac{B_{11}}{2}u_2^2 + D_{30}u_1^3 + D_{21}u_1^2u_2 + D_{12}u_1u_2^2 + D_{03}u_2^3,$$

with

$$C_{30} = -\frac{B_{30}}{2}, \quad C_{21} = \frac{B_{11}^2}{3} - \frac{B_{21}}{2} + B_{30}, \quad C_{12} = -\frac{2B_{11}^2}{3} + \frac{2B_{21}}{3} - \frac{B_{30}}{2},$$
$$C_{03} = -\frac{B_{03}}{2} + \frac{3B_{11}^2}{10} - \frac{B_{21}}{6} + \frac{B_{30}}{30}, \quad D_{30} = B_{30}, \quad D_{21} = -\frac{B_{11}^2}{2} + B_{21} - \frac{3B_{30}}{2},$$
$$D_{12} = \frac{5B_{11}^2}{6} - B_{21} + \frac{B_{30}}{2}, \quad D_{03} = B_{30} - \frac{B_{11}^2}{3} + \frac{B_{21}}{6}.$$

The quadratic terms can be simplified following the generic Bogdanov–Takens normal form reduction (see, e.g., [20, 25]), by setting

$$u_1 = \xi_1,$$
$$u_2 = \xi_2 + \frac{B_{11}}{2}\xi_1\xi_2 - \frac{B_{11}}{3}\xi_2^2,$$

multiplying the resulting flow by the scalar function $1 + B_{11}\xi_1$, and then setting

$$\xi_1 = \mu_1,$$
$$\xi_2 = \mu_2 - B_{11}\xi_1\xi_2.$$

Then, the nonresonant cubic terms are eliminated by setting

$$\mu_1 = \nu_1 + \frac{1}{36}(2B_{11}^2 - 12B_{21} + 15B_{30})\nu_1^3 + \frac{1}{12}(6B_{03} - 5B_{11}^2 + 5B_{21} - 3B_{30})\nu_1^2\nu_2,$$
$$\mu_2 = \nu_2 + \frac{B_{30}}{2} + \frac{1}{12}(13B_{11}^2 - 6B_{21} + 3B_{30})\nu_1^2\nu_2 + \frac{1}{6}(6B_{03} - 4B_{11}^2 + B_{21})\nu_1\nu_2^2$$
$$+ \frac{1}{90}(45B_{03} - 7B_{11}^2 + 15B_{21} - 3B_{30})\nu_2^3.$$

The resulting flow has equations

$$\dot{\nu}_1 = \nu_1 + \mathcal{O}(\|\nu\|^4),$$
$$\dot{\nu}_2 = B_{11}\nu_1\nu_2 + B_{30}\nu_1^3 + \left(\frac{B_{11}^2}{2} + B_{21} - 3B_{30}\right)\nu_1^2\nu_2 + \mathcal{O}(\|\nu\|^4).$$

Appendix E. Normal form reduction of the sliding vector field of a visible-invisible two-fold. The normal form (5.5) is obtained by the same means as in Appendix A, by multiplying $\tilde{f}^s$ by the quantity $(V^+ - 1/V^+)$ and then taking the dynamics along the direction $(V^+, 1)$ of the singular eigenvector. The coefficient of the second order term in (5.5) is

$$a_2 = -c_{22}^+V^+ - c_{23}^+ + c_{32}^+ + \frac{c_{33}^+}{V^+} - c_{22}^-(V^+)^2 - c_{23}^-V^+ + c_{32}^-V^+ + c_{33}^-. \tag{E.1}$$

Acknowledgment. A.C. thanks the the University of Bristol for their hospitality during much of this work.

REFERENCES

[1] A. A. Andronov, S. E. Khaikin, and A. A. Vitt, *Theory of Oscillators*, Pergamon Press, Oxford, UK, 1965.
[2] V. I. Arnold, V. V. Goryunov, O. V. Lyashko, and V. A. Vasiliev, *Dynamical Systems* VI: *Singularity Theory* I. *Local and Global Theory*, Encyclopaedia Math. Sci. 6, Springer-Verlag, Berlin, 1993.
[3] J. P. Aubin and A. Cellina, *Differential Inclusions*, Springer-Verlag, Berlin, 1984.
[4] E. Benoît, J.-L. Callot, F. Diener, and M. Diener, *Chasse au canard*, Collect. Math., 32 (1981), pp. 37–119.
[5] M. Brøns, *Bifurcations and instabilities in the Greitzer model for compressor system surge*, Math. Engrg. Indust., 1 (1988), pp. 51–63.
[6] M. Brøns and K. Bar-Eli, *Canard explosion and excitation in a model of the Belousov-Zhabotinskii reaction*, J. Phys. Chem., 22 (1991), pp. 8706–8713.
[7] A. Colombo and U. Galvanetto, *Stable manifolds of saddles in piecewise smooth systems*, CMES Comput. Model. Eng. Sci., 53 (2009), pp. 235–254.
[8] E. Conte, A. Federici, and J. P. Zbilut, *On a simple case of possible non-deterministic chaotic behavior in compartment theory of biological observables*, Chaos Solitons Fractals, 22 (2004), pp. 277–284.
[9] B. Deng, *Food chain chaos with canard explosion*, Chaos, 4 (2004), pp. 1083–1092.
[10] M. di Bernardo, C. J. Budd, A. R. Champneys, and P. Kowalczyk, *Piecewise-Smooth Dynamical Systems: Theory and Applications*, Springer-Verlag, Berlin, 2008.
[11] L. Dieci and L. Lopez, *Sliding motion in Filippov differential systems: Theoretical results and a computational approach*, SIAM J. Numer. Anal., 47 (2009), pp. 2023–2051.
[12] F. Dumortier, R. Roussarie, J. Sotomayor, and H. Zoladek, *Bifurcations of Planar Vector Fields: Nilpotent Singularities and Abelian Integrals*, Springer-Verlag, Berlin, 1991.
[13] W. Eckhaus, *Relaxation oscillations including a standard chase on French ducks*, in Asymptotic Analysis II, Lecture Notes in Math. 958, Springer, New York, 1983, pp. 449–494.
[14] A. F. Filippov, *Differential Equations with Discontinuous Righthand Sides*, Kluwer Academic Publishers, Dordrecht, The Netherlands, 1988.
[15] M. Gatto, D. Mandrioli, and S. Rinaldi, *Pseudoequilibrium in dynamical systems*, Int. J. Systems Sci., 4 (1973), pp. 809–824.
[16] M. R. Jeffrey and A. Colombo, *The two-fold singularity of discontinuous vector fields*, SIAM J. Appl. Dyn. Syst., 8 (2009), pp. 624–640.
[17] M. R. Jeffrey and S. J. Hogan, *The geometry of generic sliding bifurcations*, SIAM Rev., to appear; preprint available online from http://hdl.handle.net/1983/1658.
[18] M. Kunze, *Non-Smooth Dynamical Systems*, Lecture Notes in Math. 1744, Springer-Verlag, Berlin, 2000.
[19] Y. A. Kuznetsov, *Practical computation of normal forms on center manifolds at degenerate Bogdanov-Takens bifurcations*, Internat. J. Bifur. Chaos Appl. Sci. Engrg., 15 (2005), pp. 3535–3546.
[20] Y. A. Kuznetsov, *Elements of Applied Bifurcation Theory*, 3rd ed., Springer-Verlag, Berlin, 2004.
[21] Y. A. Kuznetsov, S. Rinaldi, and A. Gragnani, *One parameter bifurcations in planar Filippov systems*, Internat. J. Bifur. Chaos Appl. Sci. Engrg., 13 (2003), pp. 2157–2188.
[22] D. M. W. Leenaerts and W. M. G. Van Bokhoven, *Piecewise Linear Modelling and Analysis*, Kluwer Academic Publishers, Dordrecht, The Netherlands, 1998.
[23] J. D. Meiss, *Differential Dynamical Systems*, SIAM Monogr. Math. Comput. 14, SIAM, Philadelhia, 2007.
[24] J. Moehlis, *Canards for a reduction of the Hodgkin-Huxley equations*, J. Math. Biol., 52 (2006), pp. 141–153.
[25] J. Murdock, *Normal Forms and Unfoldings for Local Dynamical Systems*, Springer-Verlag, Berlin, 2003.
[26] B. Peng, V. Gaspar, and K. Showalter, *False bifurcations in chemical systems: Canards*, Philos. Trans. Phys. Sci. Engrg., 337 (1991), pp. 275–289.

[27] P. T. Piiroinen and Y. A. Kuznetsov, *An event-driven method to simulate Filippov systems with accurate computing of sliding motions*, ACM Trans. Math. Software, 34 (2008), article 13.
[28] P. Szmolyan and M. Wechselberger, *Canards in* $\mathbb{R}^3$, J. Differential Equations, 177 (2001), pp. 419–453.
[29] M. A. Teixeira, *On topological stability of divergent diagrams of folds*, Math. Z., 180 (1982), pp. 361–371.
[30] M. A. Teixeira, *Stability conditions for discontinuous vector fields*, J. Differential Equations, 88 (1990), pp. 15–29.
[31] Y. Z. Tsypkin, *Relay Control Systems*, Cambridge University Press, Cambridge, UK, 1984.
[32] Z. T. Zhusubaliyev, E. A. Soukhoterin, and E. Mosekilde, *Quasi-periodicity and border-collision bifurcations in a DC-DC converter with pulsewidth modulation*, IEEE Trans. Circuits Systems I Fund. Theory Appl., 50 (2003), pp. 1047–1057.